Università
Ca'Foscari
Venezia

Environment, Sustainable Chemistry and Technologies

Final Thesis

Ca' Foscari
Dorsoduro 3246
30123 Venezia

Synthesis of novel Group 3 and lanthanides complexes containing the ferrocenyl moiety

Supervisor
Dr. Marco Bortoluzzi

Co-Supervisor
Prof. Dr. Urška Lavrenčič Štangar

Graduand
Jacopo Segato
Matriculation Number: 823175

Academic Year
2015 / 2016

To my family, my friends
and all those who helped me
in my personal growth

1 Introduction

In recent years the interest has increased towards the synthesis and the characterization of *d/f* hetero-metal complexes in many industrial sectors. Indeed, those species can find different fields of application, such as:

- Magnetic materials[1];
- Biological environments[2], to modulate the activation characteristics of enzyme sites and for the synthesis of biologically active molecules;
- Medicine, as new 'high efficiency' contrast agents in diagnostic medicine[3], and for relaxometry studies in Magnetic Resonance Imaging (MRI);
- Luminescent compounds, which can be used in different optic systems[4,5], such as NIR (Near Infrared) amplifiers in optic fibers[6].

Due to their modular proprieties, those species offer interesting possibility to frontier technological applications, such as molecular switch[7].

Heteropolymetallic compounds are characterized by the presence of two or more metal centres from *d* and *f* blocks, which can be connected by polydentate ligands able to coordinate the metal ions selectively in specific sites. The proprieties of those complexes, besides depending upon the intrinsic characteristics of the metal ions present, are influenced by the interaction of the metals of different blocks. This may be due to the spatial proximity between the metal centres, even if the development of new molecular proprieties is usually favoured by the presence of appropriate ligands able to mediate the electronic interactions. The trivalent ions of the lanthanides series (generally Ln^{3+}) are characterized by 4*f* orbitals which possess low overlapping capacity, to the point that the formation of direct bonds M(*d*)-M(*f*) is not possible. Therefore, to obtain complexes with chemical-physic characteristics of applicative interest it is fundamental the choice of the bridging ligand, to provide a good interaction between the two metal centres.

1.1 Electronic configuration of lanthanide ions

The lanthanides (Ln) at the ground state are strongly electropositive, with reduction potentials lower than -2 V. The electronic ground state of trivalent Ln^{3+} is [Xe]$4f^n$ (n=0-14). The magnetic and the spectral behaviour of the trivalent ions of lanthanides is basically different from that of the transition elements belonging to the *d* block. The electrons of 4*f* orbitals are not involved in the coordination, and form the *inner orbitals*, therefore the electronic structure $4f^n$ of the metal centre, that is the base of the magnetic and electronic proprieties, is not significantly modify neither from the nature nor from the number of substituents present in the coordination sphere.

All the ions of the lanthanides series, excepting Lu^{3+}, exhibit unpaired electrons and are paramagnetic. In any trivalent lanthanide ion, the spin of all electrons are coupled together and vectorially added, determining the spin quantum number S (the sum of the quantum number m_s), whereas the sum of the orbital angular momenta (quantum number m_l) of each electron leads to a total orbital angular momentum, characterized by the quantum number L. The different relative orientations that the magnetic momenta L and S can take are quantized and correspond to energies very different one from each other. To describe the electronic configuration of a lanthanide S and L are therefore not sufficient, but the quantum number J must be introduced, which can vary between |S+L| and |S-L| with skips by one unit. For a certain Ln^{3+} ion numerous electronic states are possible, characterized by different values of S, L and J.

To describe the electronic configurations, a symbol is associated to each value of L (L=0: S; L=1: P; L=2: D; L=3: F; L=4: G; L=5: H; L=6: I; etc.); instead the value of the quantum number S determines the multiplicity (2S+1), indicated in superscript. The J value is indicated in subscript. The ground state is established by applying the Hund rules[8]:

- The spin multiplicity is the highest possible;
- If it is present more than a value with the same spin multiplicity, the ground state has the highest value for L;
- When the f^n configuration has $n \leq 7$, J has the lowest value for the ground state; when f^n has n>7, J has the highest value for the ground state.

The spin-orbit coupling interaction generates a huge splitting of energetic levels (SO levels) having different J values, by about thousand cm^{-1}. Two exceptions are the Sm^{3+} and Eu^{3+}

ions, which have some SO excited states close to the fundamental one and result therefore populated also a room temperature.

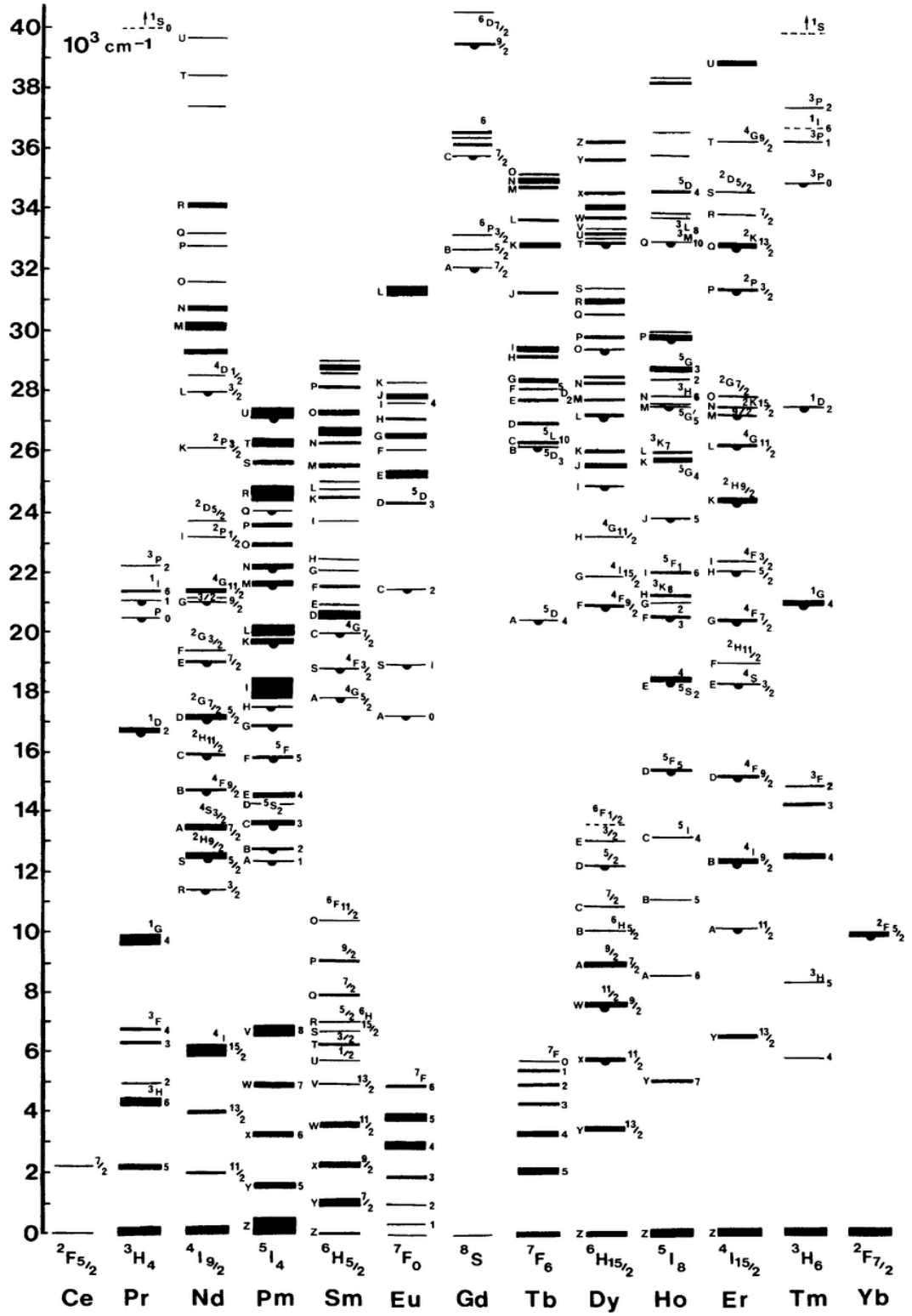

Figure 1.1: Energy level diagram for Ln(III) ions doped in a low-symmetry crystal, LaF_3.

The electrostatic influence of the ligands can lead to a further splitting of a level characterized by a certain amount of quantum numbers S, L, and J in a set of non-degenerate sublevels. Such loss of degeneration is known as Stark effect (perturbation of a $^{2S+1}L_J$ level), which is characterized by relatively low energy in Ln^{3+} complexes, typically about hundreds cm^{-1}, around an order of magnitude lower if compared to what it is commonly observable for *d* block complexes.

1.2 Luminescence of lanthanides

The luminescence, that is the physical phenomenon of emission of photon from excited materials, is one of the most interesting properties of the coordination compounds of trivalent lanthanides. The Ln^{3+} ions, characterized by partially occupied *f* orbitals, absorb electromagnetic radiation in the visible and NIR (Near Infrared) region. Laporte rule prohibits the $f \leftarrow f$ transitions (no change of orbital parity), and the coefficients of molar extinction are therefore very low, usually not above to 10 M^{-1} cm^{-1}. The frequencies of those absorptions are weakly influenced by the ligands, and changes in the coordination geometry or in the polarizability of the donor moieties rather affect the relative intensity of the $f \leftarrow f$ transitions. The poor influence of the coordinated ligands on the wavelengths and the Laporte rule obviously affect also the emissions from the excited states of trivalent lanthanide ions. In Table 1.1 are listed the main luminescence transitions of lanthanide ions that emit in the visible region.

Lanthanide ion	Transition	J value	Colour
Sm^{3+}	$^4G_{5/2} \rightarrow {}^6H_J$	J = 5/2 - 11/2	
Eu^{3+}	$^4D_0 \rightarrow {}^7F_J$	J = 0 - 6	
Tb^{3+}	$^5D_4 \rightarrow {}^7F_J$	J = 6 - 3	
Dy^{3+}	$^4F_{9/2} \rightarrow {}^6H_J$	J = 15/2 – 13/2	

Table 1.1: Main transitions of lanthanides ions in the visible region.

It is to be highlighted that some transitions of the Sm^{3+}, Eu^{3+} and Dy^{3+} ions appear at wavelength above 700 nm, *i.e.* in the near-infrared range (NIR). Ions such as Nd^{3+}, Er^{3+} and Yb^{3+} are exclusively NIR emitters. Each emission has its own intensity, which depends by selection rules principally based on ΔJ value between excited state and ground state and by the influence of the coordination sphere. In Figure 1.2 are shown the typical emissions of the Ln^{3+} ions.

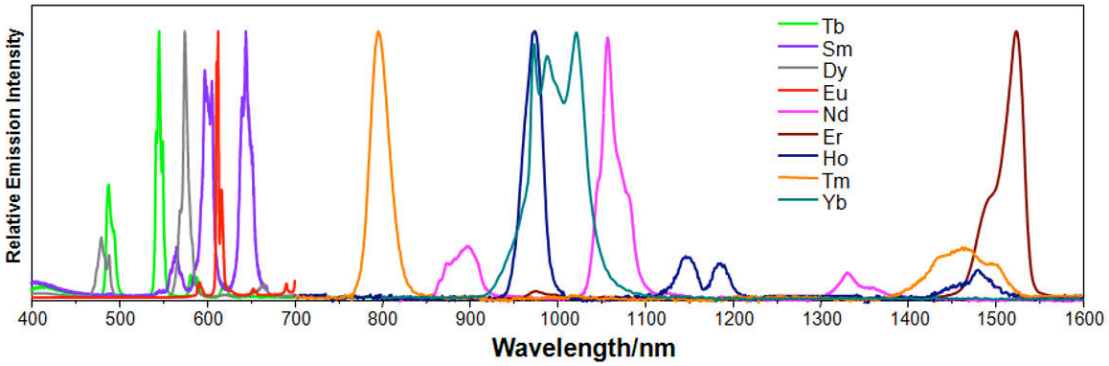

Figure 1.2: Normalized typical emission spectra of trivalent lanthanide ions.

As already highlighted, the 4*f* shell is well separated from the valence orbitals 6*s*, 6*p* and *5d*, therefore the perturbation due to the coordinated ligands is very limited and all the complexes of the same lanthanide ion show emission spectra with transitions that fall almost at the same frequencies. Both the absorption spectra and the emission spectra of the lanthanide ions consist in very thin picks, being the *f-f* transitions scarcely affected by the vibrations of the complexes. This aspect confers to the spectra a chromatic cleanliness which is completely absent in the complexes of the *d* block metals, because of the nature of the 4*f* orbitals which behave as *core* orbitals.

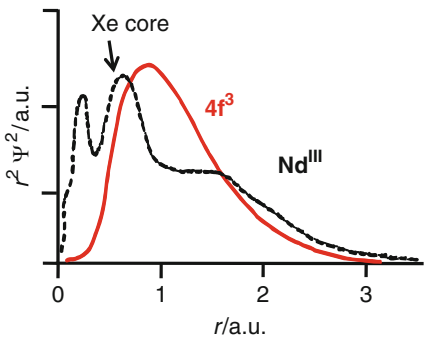

Figure 1.3: Radial wavefunction of the three 4f electrons of Nd^{III} compared with the radial wavefunction of the xenon core (a.u. = atomic units).

The lifetime of the emission of lanthanides are order of magnitude greater than the common fluorescent organic compounds or those generated by some complexes of *d* block metals[9], mainly because of the Laporte rule. This feature makes luminescent lanthanide derivatives of interest for different technological application. However, the photoluminescence of the lanthanide salts is very weak, mainly because of the very low absorption coefficients. An improvement of the intensity of the luminescence can be obtained by suitable ligands, which must possess good absorption features and the possibility to transfer the absorbed energy to the metal centre, exciting it[10]. This mechanism is known as *Antenna Effect*, depicted in Figure 1.4. The return at the ground state can take place through radiative transition *f*→*f*.

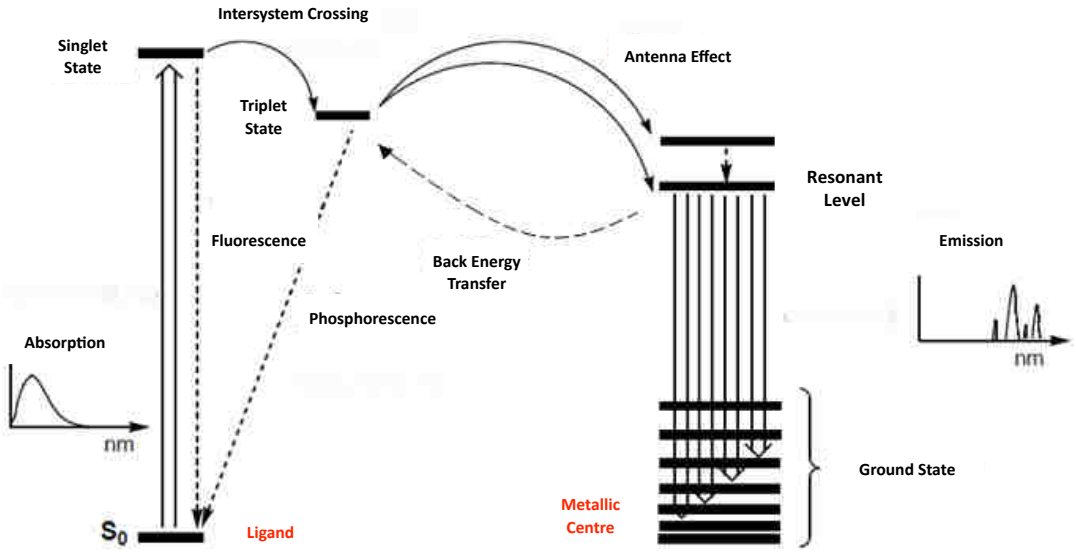

Figure 1.4: Antenna effect mechanism.

The energy transfer from the ligand to the lanthanide ion can occur with different mechanisms, the most common involving the excited triplet state of the ligand as source for the population of the emitting state of the Ln^{3+} ion. The ligand-lanthanide energy transfer can concern only a quantum of energy (Förster mechanism) or can be accompanied by ligand-lanthanide electronic exchange (Dexter mechanism). In the case of ytterbium, ligand-to-metal charge transfer affording and Yb^{2+} intermediate is sometimes proposed. The efficiency of the *Antenna Effect* depends on several factors, such as the proximity of the

antenna ligand to the metal centre and the relative energies of the ligand and lanthanide excited states. In particular, the excited levels of the coordinated ligand must be quite higher than the emitting level of the ion, otherwise a *Back Energy Transfer* can occur, with consequent quenching of lanthanide luminescence.

On the basis of the HSAB (*Hard and Soft Acids and Bases*) theory, the Ln^{3+} ions are classified as *hard* acids. For this reason, widespread antenna-ligands are chelating compounds with oxygen/nitrogen as donor atoms, classified as *hard* ligand, ideally anionic. Common organic ligands used as antenna-systems are for instance β-diketonates, dipicolinic acid derivatives, 8-hydroxiquinolinates (Figure 1.5). The behaviour as antenna of those ligands is modulated through the choice of the substituents. The coordination of *soft* donors is usually weak if it not enforced by electrostatic factors, as happens for instance in lanthanide dithiocarbamates.

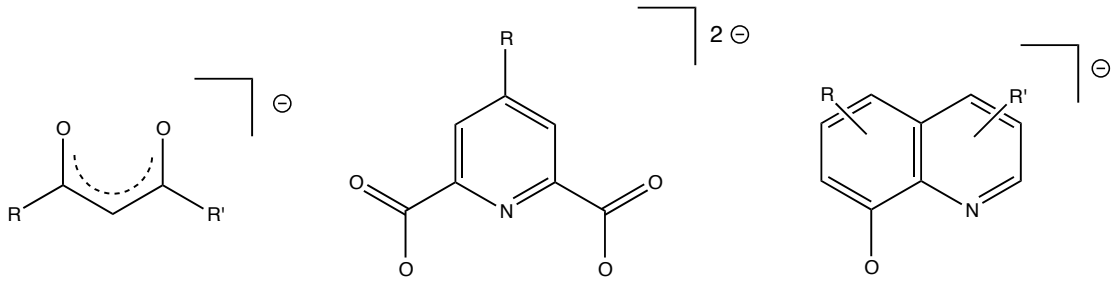

Figure 1.5: Examples of common organic antenna-ligand.

1.3 Complexes of the *d*-block elements used as antenna

Recently, with the aim of intensify and/or modulate the photoluminescence of lanthanide ions, the study of new antennae able to improve the luminescence has been oriented towards species containing elements belonging to the *d* block. Transition metals indeed have characteristics which make them interesting for their insertion into antenna-systems[11]:

- The coordination compounds of *d*-block elements can show very wide absorption spectra, from the near ultraviolet to the near infrared, especially if mechanisms of absorption such as the *Metal-to-ligand Change Transfer (MTLT)* are active;

- The excited triplet state has usually longer lifetime with respect to common organic ligand and this favours the effectiveness of the energetic transfer to the resonance levels of Ln^{3+} ions;
- The chemical and photochemical stability of many complexes of transition elements can be higher than that of common organic antenna-ligands;
- The redox proprieties of a transition element are exploitable to the creation of those which are called "Molecular Switch", that is a system able to alter its luminescence on changing the oxidation state of the metal centre[12].

Although heterometalic systems were created with basic ligands, such as the cyanide ion[13] and oxalate ion[14], particular attention has been paid to the *design* of appropriate polydentate ligands, which are able to act as a bridge. Some examples of bridging ligands are:

- Chelating nitrogen-donor, such as 2,2'-bipyrimidine (bpym) (Figure 1.6)[15], 2,3-bis(2-pyridyl)pyrazine (bppz) (Figure 1.7)[16] and 3,5-bis(2-pyridyl)pyrazolate (Figure 1.8)[17]. Further studies about ligands belonging to this category were focused on the relationship between the antenna-effect, the distance of the metal centres and the conjugation of the ligand[18];
- Nitrogen bidentate ligands functionalized with oxygen-donor groups. For instance, Faulkner et al. [19] have used a bipyridin-carboxylate to coordinate through the di-imine function a *d*-block metal (Ru^{2+} or Os^{2+}) and a lanthanide ion (Yb^{3+}, Nd^{3+}, Eu^{3+}) by the carboxylate moiety, as shown in Figure 1.9;
- Functionalized cyclen (tetrazacyclododecane) ligands. For example, in the complexes shown in Figure 1.10 the cyclen group coordinates the trivalent lanthanide, while the lateral chains containing triazole- or phenantroline-based moieties connect the other metal centres[20, 21];
- Polypyridin-acetylide ligands, an example of which has allowed to obtain modulation of photoluminescence in the NIR region of the Ru-Yb complex shown in Figure 1.11 through electrochemical tuning.

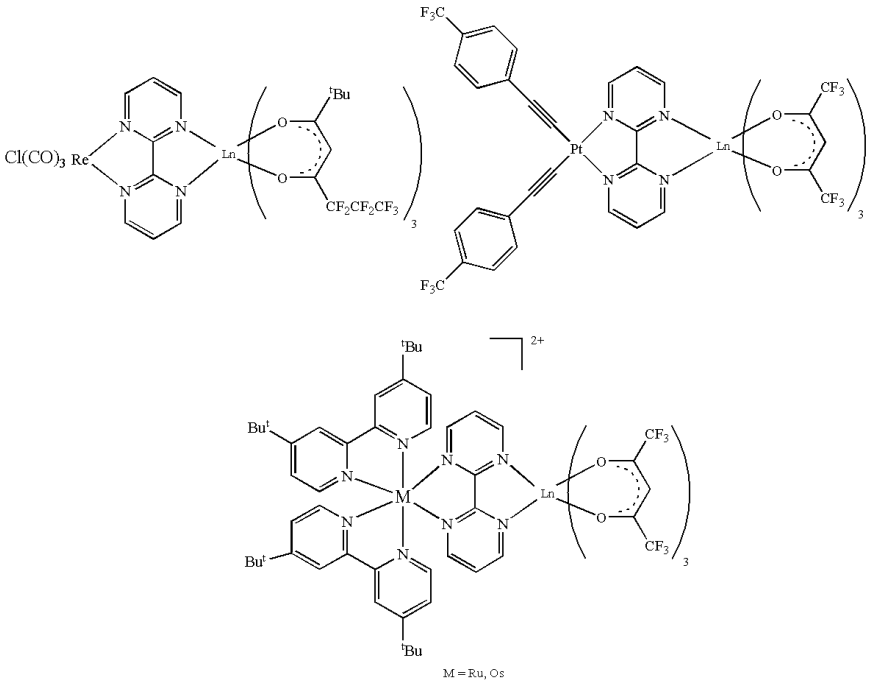

Figure 1.6: Bimetallic complexes: $(C_9H_4F_3)Pt(bpym)Ln(dike)_3$, $(CO)_3ClRe(bpym)Ln(dike)_3$ and $[M(^tBu_2Bipy)_2Ln(dike)_3][PF_6)_2$.

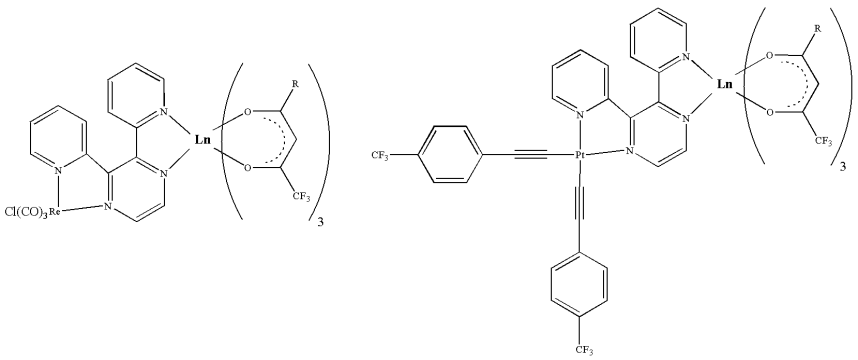

Figure 1.7: Heterobimetallic complexes Re-Ln and Pt-Ln with the bppz ligand.

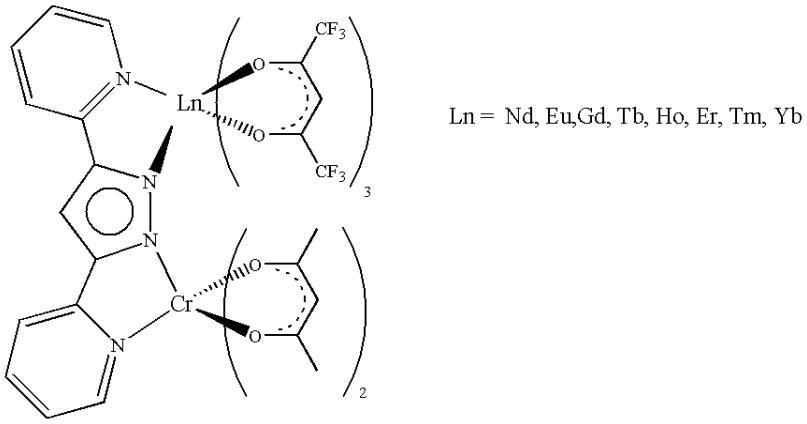

Figure 1.8: Cr-Ln complexes with the 3,5-bis(2-pyridyl)pyrazolate bridge.

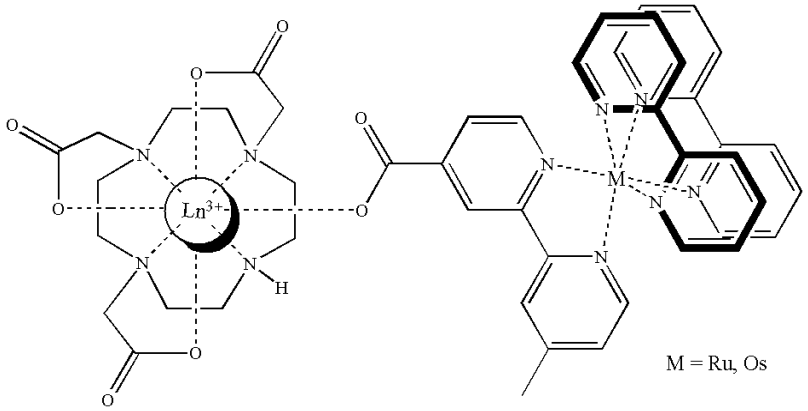

Figure 1.9: Ru/Os-Ln system with 4-carboxylbipyridine.

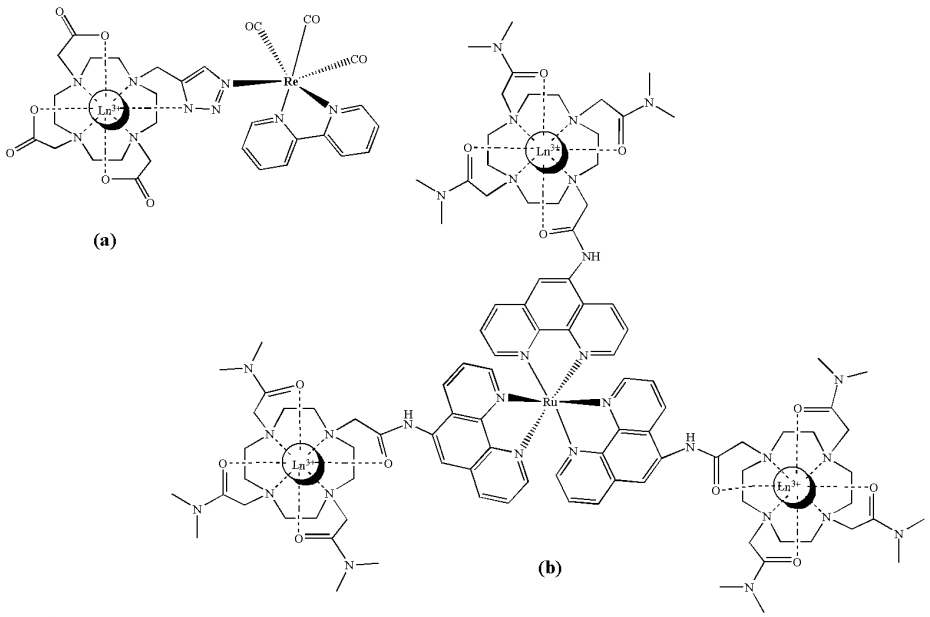

Figure 1.10: Heteropolymetallic *d/f* complexes synthesized by Faulkner and co. (a) Re-Ln complex; (b) Ru-Ln_3 complex.

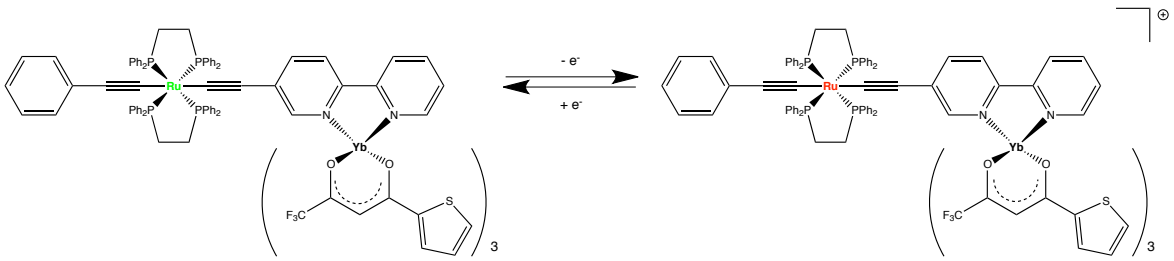

Figure 1.11: Reversible redox process of the couple Ru(II)/Ru(III) in the Ru-Yb complex.

Antenna-systems containing elements of *d* block able to increase the lanthanide luminescence in the visible region are rarer than NIR emitters. The team of De Cola has used the benzoic acid as ligand, previously substituted in *para* position with a pyridine-triazole moiety, able to coordinate through two nitrogen atoms one centre of iridium(III) and with a carboxylate group a europium ion. The Ir_2-Eu complex obtained, show in Figure 1.12, is the first example of trimetallic complex *d/f* showing a globally emission of white colour, which it is of great technological interest[22].

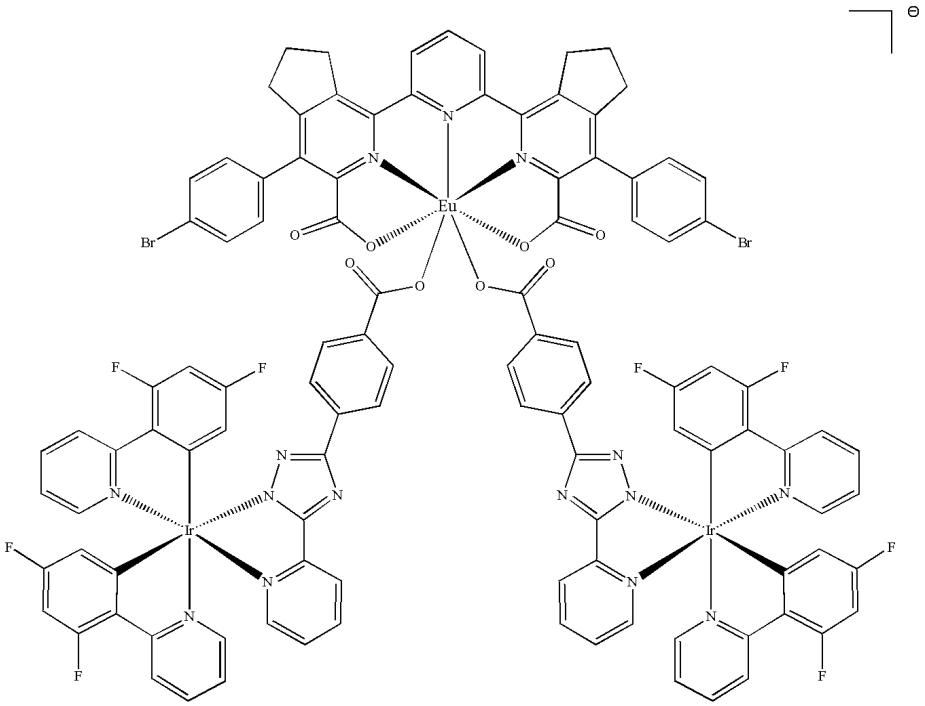

Figure 1.12: Heterotrimetallic complex Ir_2-Eu.

The research team of Huang has used as bridging ligand the 4,4,5,5,5-pentafluoro-1-(1',10'-phenanthrolin-2'-il)-penta-1,3-dionate, which has been coordinated to an iridium(III) metal

centre through the nitrogen atoms of the phenanthroline moiety. The presence of the β-diketone fragments has allowed to synthesise the Ir_3-Eu complex shown in Figure 1.13, which is an efficient emitter in the red region[23].

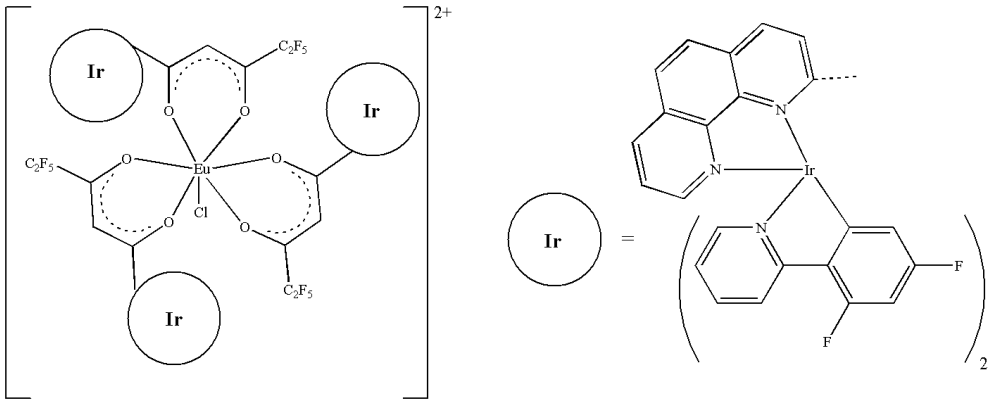

Figure 1.13: Heterotetrametallic complex Ir_3-Eu.

The joint emissions of Eu^{3+} ion and Ir(III) fragments with [*N,C*] ligands derived from the 2-phenylpyridine skeleton is still of actual interest for the preparation of compounds having globally white emission. For example, Baschieri, Sambri and co-workers reported in 2015 a series of trimetallic Ir_2Eu compounds where the bridging ligands coordinate the lanthanide ion by a β-diketonate moiety and the iridium centre by a isocyanide fragment (see Figure 1.14)[24].

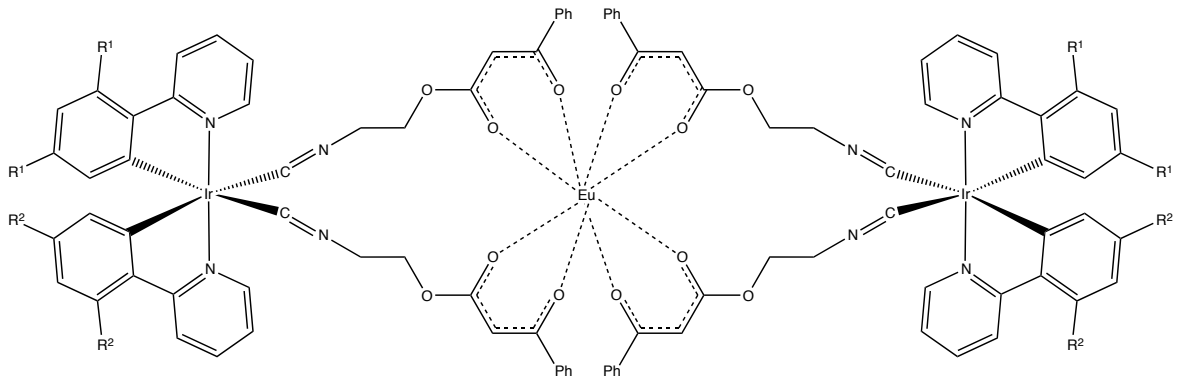

1: $R^1=R^2=H$
2: $R^1=H$; $R^2=F$
3: $R^1=R^2=F$

Figure 1.14: Heterotrimetallic complex Ir_2-Eu with β-diketonate-isocyanide ligand.

1.4 Ferrocene-based antenna-ligands

Several lanthanide complexes containing the ferrocene moiety are reported in the literature[25], which sometimes found application as precursors for mixed oxides or as polymerization catalysts[26]. Few examples of luminescent species are however known.

The coordination to the Eu^{3+} ion of a phenanthroline ligand functionalized with ethynyl-ferrocene groups has allowed to obtain the tri-metallic derivative represented in Figure 1.15, which exhibits emission due to the lanthanide ion in the red region[27].

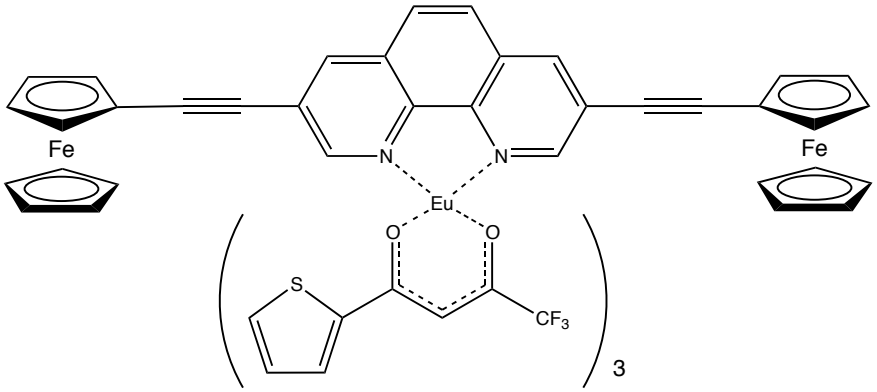

Figure 1.15: Structure of the complex $[Eu(tta)_3(Fc_2phen)]$.

An example of molecular switch in the visible region is represented in Figure 1.16[28]. The luminescence is modulated through the redox couple ferrocene/ferricinium. The luminescence of the complex, made up of emission bands $^5D_O \rightarrow {}^7F_J$ between 575 and 725 nm associated to emission from the europium centre, undergoes a reversible modulation of intensity on the changing of the oxidation state of iron.

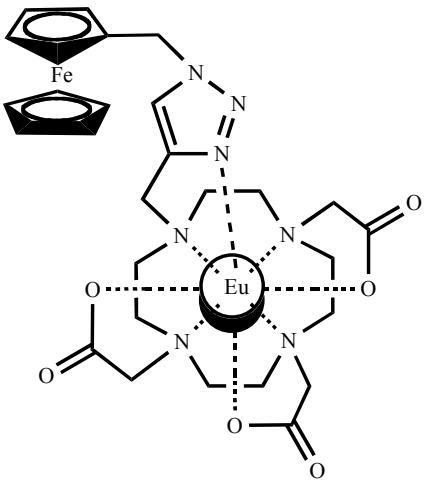

Figure 1.16: Molecular switch Fe-Eu.

1.5 Aim of the thesis

The purpose of this thesis is the synthesis and the characterization of new hetero-metallic complexes of elements belonging the *d*-block and the lanthanide series. The research work is mainly based on the preparation of complexes containing ferrocene-functionalized molecules as antennae. The lanthanide centres will be chosen on the basis of their emission features. Particular interest will be devoted to the visible-emitting Eu^{3+} ion and the NIR-emitting Yb^{3+} ion. The coordination chemistry studies will be extended to the diamagnetic Y^{3+} ion to make NMR some characterizations easier. The redox behaviour of the new ferrocene-containing ligands and complexes will be deeply investigated.

2 Experimental part

2.1 Instrumentation

The reaction conducted under inert atmosphere (O_2 < 5 ppm, H_2O < 1 ppm) were carried out inside a MBraun *glove box* provided with purifier and automatic pressure control and equipped with the common instrumentation for inorganic synthesis. The spectra in the medium infrared region were collected employing a Perkin-Elmer *SpectrumOne* spectrometer in the range 4000 – 400 cm^{-1}. The samples were previously dispersed and homogenized in KBr. The absorption spectra of solutions of samples were recorded using a Perkin-Elmer *Lambda 40* spectrophotometer in a range between 220 and 1100 nm. The emission features of solid samples of the new compounds were studied at room temperature in the range 400 – 1050 nm, using an OceanOptics *Flame T* spectrometer, coupled with an optical fibre, a collimating achromatic lens and a longpass (> 395 nm) filter. Two UV led sources, having emission peaks at 375 and 280 nm respectively, were used to excite the samples. The nuclear magnetic resonance (NMR) spectra were collected at different temperatures by the use of Bruker Ascend 400 and Bruker Avance 300 spectrometers, operating at 400.13 MHz and 300.13 MHz proton frequency, respectively. The samples were prepared dissolving the complexes in $CDCl_3$ or DMSO-d_6. The partially deuterated fraction of the solvent was used as an internal standard reference, itself referred to tetramethylsilane (TMS). Standard sequences were used to record bi-dimensional spectra and for diffusion (DOSY) experiments. The calibration of DOSY experiments was done with a 5% H_2O sample in D_2O. To avoid the influence of convective phenomena the temperature control was turned off during the DOSY experiments. Every measure was preceded by the optimization of the diffusion time (Δ) and the duration (δ) of the gradient of the magnetic field (g). The data were processed to obtain the diffusion coefficient (D) both through transformation in pseudo-bidimensional spectra, and carrying out exponential interpolation on the variation of peak intensity (I) as a function of the square of the gradient of the magnetic field, on the basis of the equation $I = I_0 \exp[-D\gamma^2 g^2 \delta^2(\Delta - \delta/3)]$ (γ = gyromagnetic ratio[29]).

The electrochemical measurements were conducted using an electrochemical cell having a three electrodes configuration (working, reference and counter electrodes). A platinum micro-electrode (12.5 μm of radius) was the working electrode. The reference electrode was Ag/AgCl saturated with KCl, and the counter electrode was a spiral of platinum. The cells were introduced in an aluminium Faraday cage to eliminate the interferences due to external electrostatic fields. The electrical contacts were made with shielded cables. The voltammetric measurements were performed using a potentiostat/galvanostat CH Instruments model 760B, operated by CHI760B software (CH Instrument).

DFT calculations on model systems were carried out using the hybrid functional EDF2[30] in combination with the split-valence polarized basis set 6-31G***[31]. The "unrestricted" approach was applied for compounds having unpaired electrons and the lack of spin contamination was verified by comparing the $<S^2>$ values with the theoretical ones[32]. The software used was Spartan '16[33], running on Intel-based X86-64 workstations.

2.2 Reagents and solvents

The anhydrous chlorides and triflates of yttrium and lanthanides used are product by Strem. All those species were handled without any further purification. The other reagents, acids, bases, and the salts were purchased from Sigma Aldrich or VWR International and used without further purification. The solvents for the syntheses and the electrochemical measurements were anhydrified and purified following standard methods and stored under inert atmosphere[34]. The deuterated solvents for NMR spectroscopy are Euriso-Top products.

2.3 Synthesis of ligands

2.3.1 Synthesis of potassium 1-ferrocenyl-1,3-butanedionate K[FcCOCHCOCH$_3$]

The synthesis was conducted in two steps:

1. Synthesis of the neutral β-diketone:

Inside glovebox: 2.5 g of acetylferrocene (11 mmol) are dissolved in THF in a 100 mL flask. 1.35 g of potassium *tert*-butoxide (K[O^{t}Bu]) are added to the solution. After 10 minutes a brown solid begins to precipitate. 30 minutes later 5 mL of ethyl acetate are added drop-by-drop, and the solution is let to react overnight at room temperature.

The flask is taken out of the box and the reaction quenched with slightly acidic water. The product is extracted with diethyl ether and anhydrified with magnesium sulphate. Finally, the solution is filtered and the ethyl ether is evaporated. The solid formed is a mixture of the reagent and the desired product with a ratio 1:1.3, as checked by ^{1}H NMR spectroscopy.

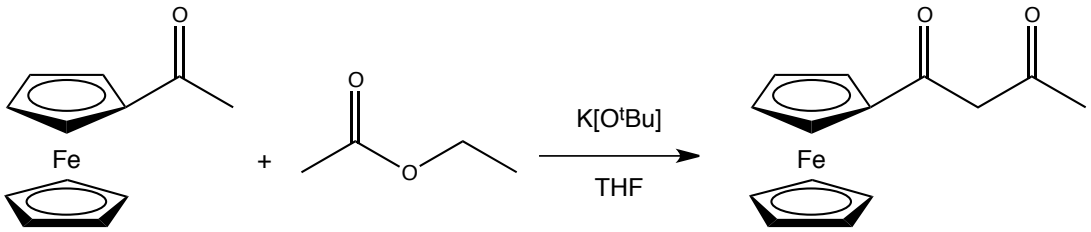

Scheme 2.1: Synthesis of $FcCOCH_2COCH_3$.

2. Synthesis of the potassium salt:

Inside the glovebox: 0.5 g of the crude product is dissolved in THF and 0.13 g of K[O^{t}Bu] is added. The reaction is completed in 8 h. The solid product which separated out is filtered, washed with diethyl ether, filtered and dried. Global yield (calculated on acetylferrocene): 50%.

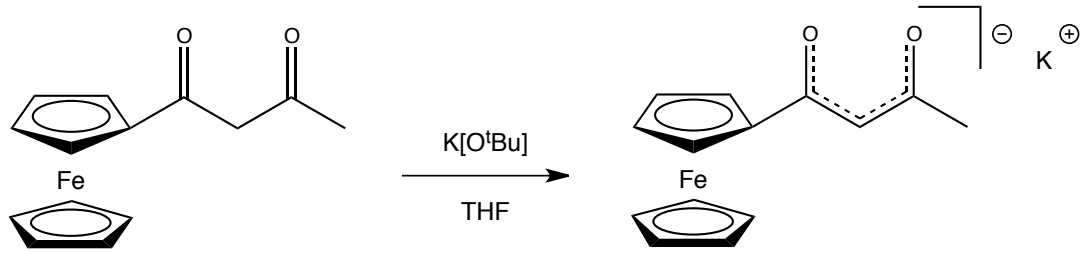

Scheme 2.2: Synthesis of $K[FcCOCHCOCH_3]$.

2.3.2 Synthesis of ferrocenecarboxylic acid FcCOOH

The synthesis of ferrocenecarboxylic acid was conducted through oxidation of the acetylferrocene with potassium hypochlorite, following a method reported in the literature[35]. The KOCl solution was prepared immediately prior to synthesis by disproportion of Cl_2 in aqueous KOH. The gaseous chlorine was obtained *in situ* from the reaction of concentrated HCl and MnO_2.

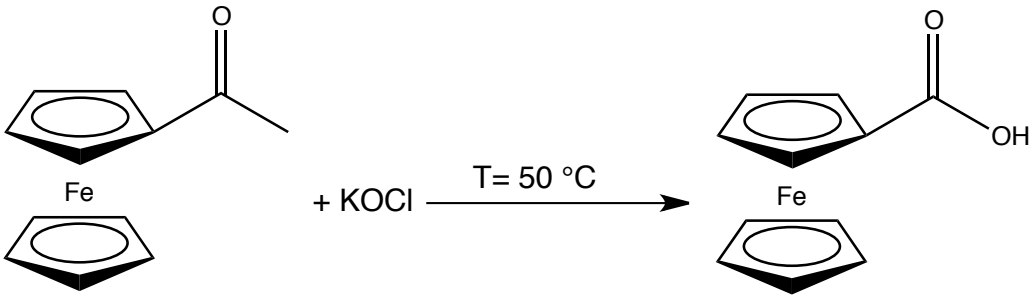

Scheme 2.3: Sythesis of FcCOOH.

In a 500 mL three-necked flask provided with a bubble condenser and a thermometer to check the temperature, 125 mL of potassium hypochlorite (15.4 % w/w) and 5.70 g (25.00 mmol) of acetylferrocene are introduced. The reaction mixture is warmed up to 50 °C and vigorously stirred. Further amounts of potassium hypochlorite solution, each of 62.5 mL, are added after 90, 120 and 180 minutes, then solution is left under stirring other 2 hours. After purification by filtration, to the solution is slowly added sodium metabisulfite (52.44 g) to neutralize the excess of oxidant. Finally, the solution is acidified with HCl until the formation of a yellow precipitate. The solid is dried under reduced pressure and characterized. Yield: 48%.

2.3.3 Synthesis of ferrocenecarboxylic acid ethyl ester FcCOOEt

Inside glovebox: 200 mg (0.868 mmol) of ferrocenecarboxylic acid is dissolved in toluene in a 50 mL flask. An equimolar amount of phosphorous pentachloride (181 mg) is slowly added. The solution tends to darken. After a couple of hours, the solvent and the by-product $POCl_3$ are removed by evaporation under reduced pressure. The solid formed is dissolved in

ethanol which acts also as reactant, and let to react overnight. The alcoholic solution is evaporated before taking out the flask from the box. Water is added and the ester is extracted with diethyl ether. After anhydrification and filtration, the solid product is collected by evaporation of the solvent under reduced pressure and finally characterized. Yield: 67%.

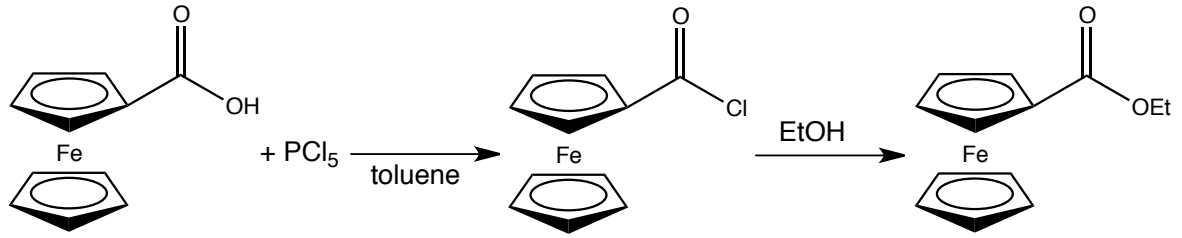

Scheme 2.4: Synthesis of FcCOOEt.

2.3.4 Synthesis of bis(diphenylphosphinoferrocene) dioxide $Fc(PPh_2O)_2$

0.5 g of bis(diphenylphosphino)ferrocene is dissolved in 10 mL of benzene. 0.5 mL of hydrogen peroxide (ca. 11 M) are slowly added. After 10 minutes the formation of a yellowish precipitate is observed. The solution is stirred for 30 minutes, then the solid is filtered on gooch, washed with benzene and dried under vacuum. Yield: 95%

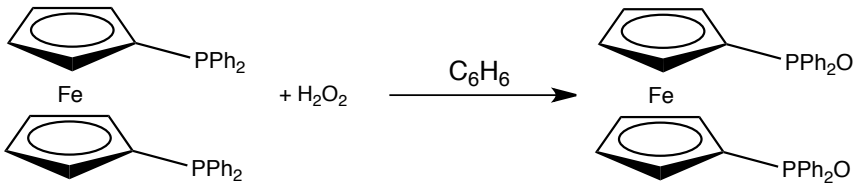

Scheme 2.5: Synthesis of $Fc(PPh_2O)_2$.

2.3.5 Synthesis of potassium tris(3,5-dimethyl-pyrazol-1-yl)borate $K[Tp^{Me2}]$

The ligand was synthesized following the method proposed by Trofimenko[36], shown in Scheme 2.6.

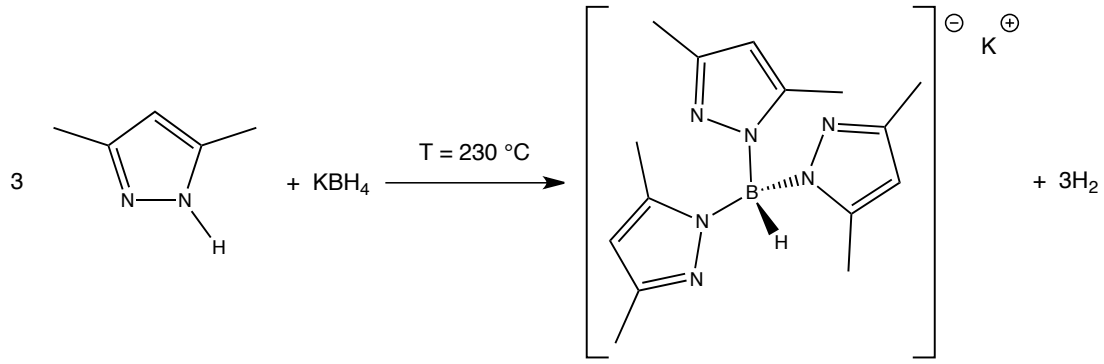

Scheme 2.6: Synthesis of K[Tp^{Me2}].

In a 25 mL flask are introduced 540 mg (10.00 mmol) of potassium borohydride and 4.80 g (50.00 mmol) of 3,5-dimethylpyrazole. The mixture is taken to the melting point and then slowly heated up to about 200°C. During the reaction the production of hydrogen is monitored, at the end of which (after about 3 hours) the reaction mixture is allowed to cool down to 130 °C and decanted into 20 mL of toluene. After cooling to room temperature, the white solid obtained is filtered, washed with diethyl ether and dried under vacuum. Yield ≥ 70%

2.3.6 Synthesis of sodium nitromalonaldehyde monohydrate Na[NMA]·H_2O

The synthesis was conducted according to a known method in the literature[37]. In a 200 mL flask 25.8 g (0.374 mol) of sodium nitrite are dissolved in 25 mL of distilled water. The solution is stirred and warmed up to 50 °C until the complete solubilisation of the solid. In the whole period of two hours a solution of mucobromic acid (25.8 g, 0.100 mol) in ethanol (25 mL) is added drop-by-drop. At the end of the addition the solution is maintained at about 54 °C for 10 minutes under stirring, then it is cooled down with a water-ice bath. The yellowish-orange precipitate is collected by filtration. The raw product is moved into a flask and dissolved in 40 mL of ethanol 95% and 10 mL of distilled water. The solution is heated to boiling and then filtered to remove a yellow by-product. The clear solution thus obtained is cooled down with an ice bath. The pink product is separated by filtration and dried under vacuum. Yield: 40%.

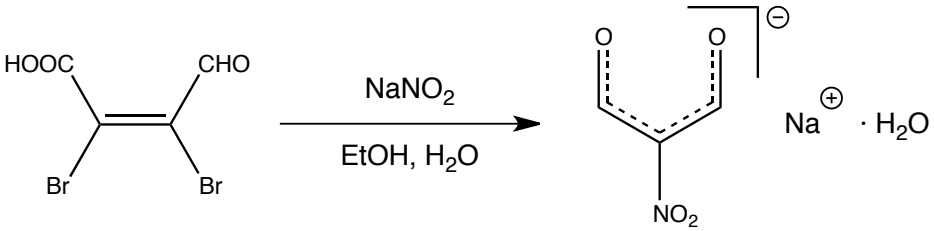

Scheme 2.7: Synthesis of Na[NMA]·H_2O.

2.3.7 Synthesis of sodium bromomalonaldehyde Na[BrMA]

The synthesis was conducted according to a known method[38]. In a 100 mL flask 5 mL (30 mmol) of 1,1,3,3-tetramethoxypropane are dissolved in 5 mL of distilled water. The solution is kept under stirring and 37% hydrochloric acid (0.21 mL) is added. When the solution becomes transparent 30 mmol of Br_2 are slowly added. After few minutes, the yellowish solution is concentrated at reduced pressure and the solid formed is filtrated, washed with cold ethanol and dried under vacuum. Yield: 70%.

The bromomalonaldehyde (30 mmol) is allowed to react with an equivalent of water solution of sodium hydroxide (30 mL of solution 1M). The solution is then concentrated to reduced pressure to few mL and diluted with acetone until the separation of a solid, which is collected by filtration and dried under vacuum. Yield: 95%.

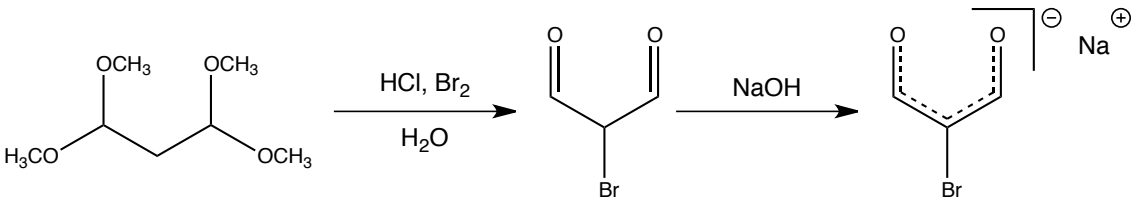

Scheme 2.8: Synthesis of Na[BrMA].

2.4 Synthesis of the new complexes

2.4.1 Synthesis of $Ln(FcCOCHCOCH_3)_3$ (Ln = Y, Eu, Yb)

Inside glovebox: in a 50 mL flask 0.1 mmol of the proper anhydrous triflate $Ln(SO_3CF_3)_3$ and 0.3 mmol (95 mg) of K[$FcCOCHCOCH_3$] are dissolved in THF and allowed to react overnight at

room temperature. THF is evaporated and the residual solid dissolved in CH_2Cl_2. The solution is centrifuged to eliminate the by-products. The supernatant is collected in a new flask and the solvent is evaporated under reduced pressure. The solid is triturated with n-hexane, filtered and dried under vacuum. Yield: 55~57%

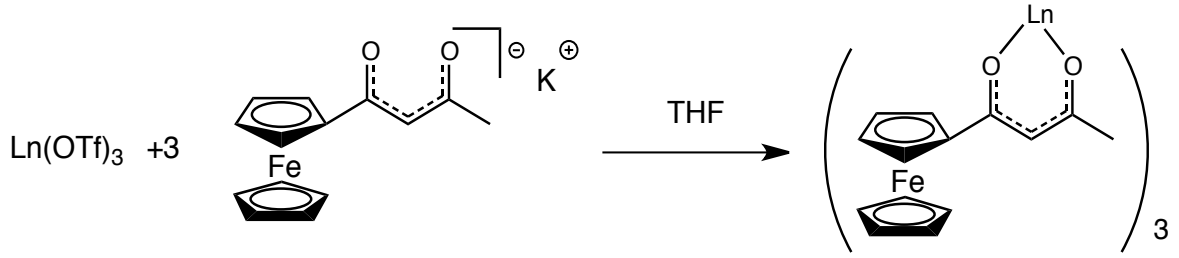

Scheme 2.9: Synthesis of $Ln(FcCOCHCOCH_3)_3$.

Characterization of $Y(FcCOCHCOCH_3)_3$

Elemental analysis: theoretical: C= 57.05%, H= 4.90%; found: C= 56.89%, H= 4.92%.

IR (KBr): 1570 cm^{-1} $\nu_{(COCHCO)}$, 1520 cm^{-1} $\nu_{(COCHCO)}$.

^{1}H NMR (DMSO-d_6, 338 K, δ): 5.77 (s, 1H, *FcCOCHCOCH₃*); 4.74 (s, 2H, *Fc*); 4.36 (s, 2H, *Fc*); 4.15 (s, 5H, *Fc*); 1.95 (s, 3H, *FcCOCHCOCH₃*).

UV-vis (CH_2Cl_2, 298 K, nm): <630, max 316 (ε = 21300 M^{-1} cm^{-1}); max 462 (ε = 2600 M^{-1} cm^{-1}).

Characterization of $Eu(FcCOCHCOCH_3)_3$

IR (KBr): 1570 cm^{-1} $\nu_{(COCHCO)}$, 1520 cm^{-1} $\nu_{(COCHCO)}$.

^{1}H NMR (DMSO-d_6, 298 K, δ): 4.28 (s, 5H, *Fc*); 4.27 (s, 2H, *Fc*); 3.55 (s, 2H, *Fc*); -0.36 (s, 3H, *FcCOCHCOCH₃*); -2.04 (s, 1H, *FcCOCHCOCH₃*).

Characterization of $Yb(FcCOCHCOCH_3)_3$

IR (KBr): 1572 cm^{-1} $\nu_{(COCHCO)}$, 1518 cm^{-1} $\nu_{(COCHCO)}$.

2.4.2 Synthesis of $Ln(FcCOCHCOCH_3)_3(phen)$ (Ln = Y, Eu, Yb; phen = 1,10-phenanthroline)

Inside glovebox: in a flask 0.125 mmol of $Ln(FcCOCHCOCH_3)_3$ and an equimolar amount of 1,10-phenanthroline (23 mg) are dissolved in dichloromethane and let to react overnight.

The solvent is evaporated and then the solid is dispersed in diethyl ether. The product is collected by filtration and dried under vacuum. Yield: 76~80%

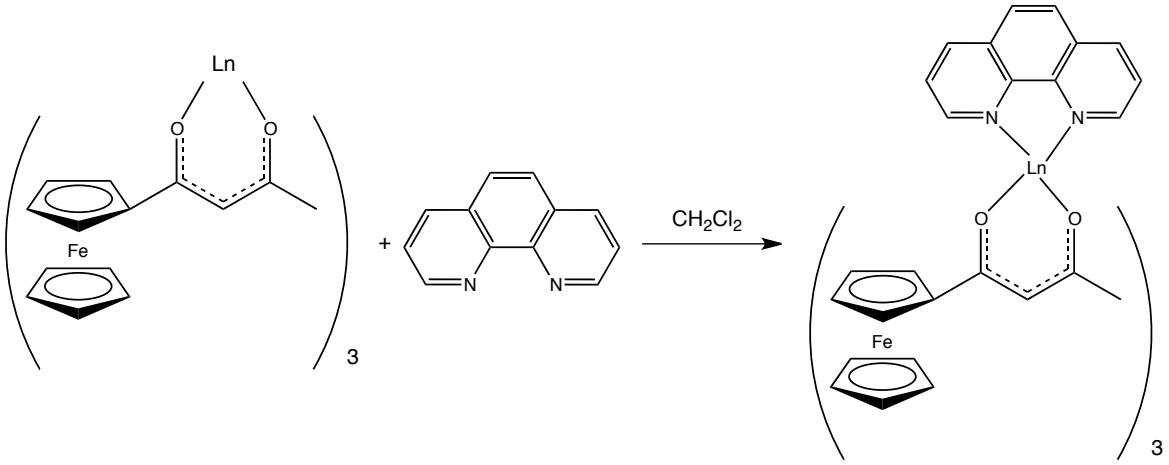

Scheme 2.10: Synthesis of $Ln(FcCOCHCOCH_3)_3(phen)$.

Characterization of $Y(FcCOCHCOCH_3)_3(phen)$

Elemental analysis: theoretical: C= 60.79%, H= 4.83%, N= 2.53%; found: C= 56.89%, H= 4.92% N= 2.49%.

IR (KBr): 1575 cm^{-1} $\nu_{(COCHCO)}$, 1515 cm^{-1} $\nu_{(COCHCO)}$.

^{1}H NMR (DMSO-d_6, 298 K, δ): 9.26 (s, br, 2H, *phen*); 8.58 (s, br, 2H, *phen*); 8.05 (s, slightly br, 2H, *phen*); 7.89 (s, br, 2H, *phen*); 5.78 (s, 3H, *FcCOCHCOCH$_3$*); 4.90 - 3.85 (m, br, 27H, *Fc*); 1.96 (s, 9H, *FcCOCHCOCH$_3$*).

UV-vis (CH_2Cl_2, 298 K, nm): <510, max 265 (ε = 38000 M^{-1} cm^{-1}); max 321 (ε = 17860 M^{-1} cm^{-1}); max 457 (ε = 870 M^{-1} cm^{-1}).

Characterization of $Eu(FcCOCHCOCH_3)_3(phen)$

IR (KBr): 1570 cm^{-1} $\nu_{(COCHCO)}$, 1520 cm^{-1} $\nu_{(COCHCO)}$.

^{1}H NMR (DMSO-d_6, 363 K, δ): 9.28 (s, br, 2H, *phen*); 8.72 (s, br, 2H, *phen*); 8.21 (s, br, 2H, *phen*); 7.91 (s, br, 2H, *phen*); 4.07 (s, br, 21H, *Fc*); 3.75 (s, br, 6H, *Fc*); 0.68 (s, br, 9H, *FcCOCHCOCH$_3$*); -0.78 (s, br, 3H, *FcCOCHCOCH$_3$*).

Characterization of $Yb(FcCOCHCOCH_3)_3(phen)$

IR (KBr): 1577 cm^{-1} $\nu_{(COCHCO)}$, 1516 cm^{-1} $\nu_{(COCHCO)}$.

2.4.3 Synthesis of $Ln(FcCOCHCOCH_3)(Tp^{Me2})_2$ (Ln = Y, Eu, Yb; Tp^{Me2} = tris(3,5-dimethyl-pyrazol-1-yl)borate)

Inside glovebox: 0.25 mmol of the proper lanthanide triflate salt and 0.5 mmol (170 mg) of potassium salt of tris(3,5-dimethyl-pyrazol-1-yl)borate), $K[Tp^{Me2}]$, are allowed to react for 4 hours in THF. To the reaction mixture is then slowly added $K[FcCOCHCOCH_3]$ (0.25 mmol, 76 mg). After 3 hours the solvent is evaporated and the residual solid is dissolved in dichloromethane. The solution is centrifuged and the supernatant is collected. After evaporation under reduced pressure, the product is dispersed in hexane, filtered and dried under vacuum. Yield: 63~67%

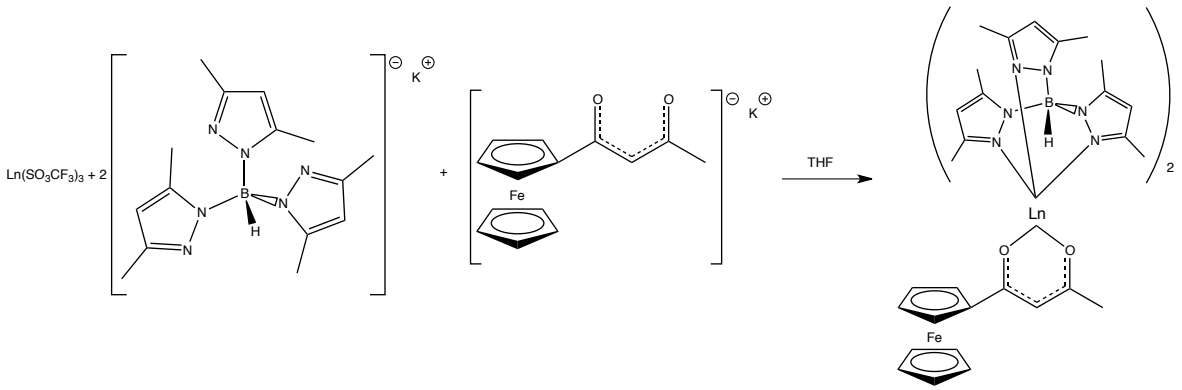

Scheme 2.11: Synthesis of $Ln(FcCOCHCOCH_3)(Tp^{Me2})_2$.

Characterization of $Y(FcCOCHCOCH_3)(Tp^{Me2})_2$

Elemental analysis: theoretical: C= 61.59%, H= 6.78%, N=19.15%; found: C= 61.09%, H= 6.82%, N=19.53%.

IR (KBr): 2545 cm^{-1} $\nu_{(BH)}$, 1576 cm^{-1} $\nu_{(COCHCO)}$, 1545 cm^{-1} $\nu_{(COCHCO)}$, 1520 cm^{-1} $\nu_{(COCHCO)}$.

^{1}H NMR (DMSO-d_6, 298 K after 350 K heating, δ): 5.79 (s, 3H, *pyrazole-H_4*); 5.76 (s, 1H, *FcCOC<u>H</u>COCH$_3$*); 5.74 (s, 3H, *pyrazole-H_4*); 4.75 (pseudo-t, 2H, J_{HH} = 1.8 Hz, *Fc*); 4.36 (pseudo-t, 2H, J_{HH} = 1.8 Hz, *Fc*); 4.14 (s, 5H, *Fc*); 2.16 (s, br, 18H, *pyrazole-Me*); 2.09 (s, br, 18H, *pyrazole-Me*); 1.94 (s, 3H, *FcCOCHCOC<u>H</u>$_3$*).

UV-vis (CH_2Cl_2, 298 K, nm): <600, max 324 (ε = 35460 M^{-1} cm^{-1}); max 466 (ε = 4230 M^{-1} cm^{-1}).

Characterization of $Eu(FcCOCHCOCH_3)(Tp^{Me2})_2$

IR (KBr): 2545 cm^{-1} $\nu_{(BH)}$, 1576 cm^{-1} $\nu_{(COCHCO)}$, 1545 cm^{-1} $\nu_{(COCHCO)}$, 1520 cm^{-1} $\nu_{(COCHCO)}$.

Characterization of Yb(FcCOCHCOCH$_3$)(Tp^{Me2})$_2$

IR (KBr): 2558 cm^{-1} $\nu_{(BH)}$, 1575 cm^{-1} $\nu_{(COCHCO)}$, 1538 cm^{-1} $\nu_{(COCHCO)}$, 1511 cm^{-1} $\nu_{(COCHCO)}$.

2.4.4 Synthesis of Ln(NMA)$_3${Fc(PPh$_2$O)$_2$} (Ln = Y, Eu, Yb; NMA = conjugate base of nitromalonaldehyde)

The proper chloride $LnCl_3$ (0.25 mmol) is dissolved in 5 mL of water, then 0.75 mmol (118 mg) of the sodium salt of nitromalonaldehyde, Na[NMA]·H_2O, previously dissolved in 7 mL of water, is slowly dripped into the solution and let to react for 2 h. Fc(PPh$_2$O)$_2$ is dissolved in 25 mL of ethanol and then added to the water solution. After allowing the mixture to react overnight at room temperature, the solid formed is filtered, washed with ethanol and dried under vacuum. Yield: 78~81%

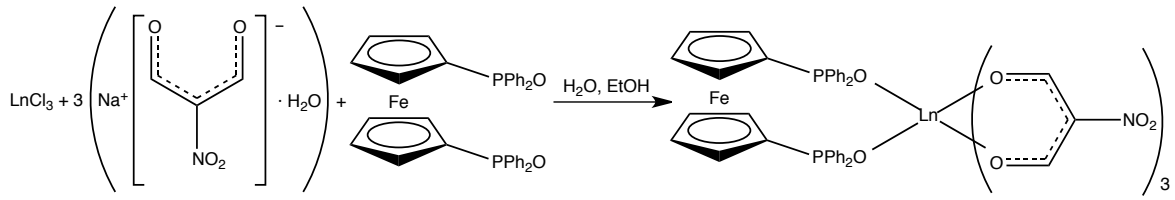

Scheme 2.12: Synthesis of Ln(NMA)$_3${Fc(PPh$_2$O)$_2$}.

Characterization of Y(NMA)$_3${Fc(PPh$_2$O)$_2$}

Elemental analysis: theoretical: C= 50.31%, H= 3.63%, N= 4.09%; found: C= 50.52%, H= 3.61%, N= 3.99%.

IR (KBr): 1650 cm^{-1} $\nu_{(CO)}$, 1507 cm^{-1} $\nu^{as}_{(NO2)}$, 1317 cm^{-1} $\nu^{s}_{(NO2)}$, 1152 cm^{-1} $\nu_{(P=O)}$.

^{1}H NMR ($CDCl_3$, 298 K, δ): 9.41 (s, 6H, *NMA*); 7.80 - 7.40 (m, 20H, *Ph*); 4.93 (s, 4H, *Fc*); 4.28 (s, 4H, *Fc*).

^{31}P {^{1}H} NMR ($CDCl_3$, 298 K, δ): 36.4 ($^2J_{PY}$ = 9.8 Hz).

UV-vis (CH_2Cl_2, 298 K, nm): <390, max 298 (ε = 19180 M^{-1} cm^{-1}); max 433 (ε = 135 M^{-1} cm^{-1}).

Characterization Eu(NMA)$_3${Fc(PPh$_2$O)$_2$}

IR (KBr): 1650 cm^{-1} $\nu_{(CO)}$, 1507 cm^{-1} $\nu^{as}_{(NO2)}$, 1317 cm^{-1} $\nu^{s}_{(NO2)}$, 1153 cm^{-1} $\nu_{(P=O)}$.

^{1}H NMR ($CDCl_3$, 298 K, δ): 10.43, 9.07, 7.75 (s, br, 20H, *Ph*); 4.06, 3.23 (s, br, 8H, *Fc*); -14.71 (s, br, 6H, *NMA*).

^{31}P {^{1}H} NMR ($CDCl_3$, 298 K, δ): 27.8 br.

Characterization of Yb(NMA)$_3${Fc(PPh$_2$O)$_2$}

IR (KBr): 1648 cm^{-1} $\nu_{(CO)}$, 1508 cm^{-1} $\nu^{as}_{(NO2)}$, 1316 cm^{-1} $\nu^{s}_{(NO2)}$, 1154 cm^{-1} $\nu_{(P=O)}$.

^{1}H NMR ($CDCl_3$, 298 K, δ): 15.72 (s, br, 6H, *NMA*); 9.70 (s, 12H, *Ph*); 8.92 (s, 8H, *Ph*); 0.82 (s, br, 4H, *Fc*); -1.85 (s, br, 4H, *Fc*).

^{1}H NMR ($CDCl_3$, 313 K, δ): 15.06 (s, br, 4H, *NMA*); 9.54 (s, 12H, *Ph*); 8.86 (s, 8H, *Ph*); 1.50 (s, 4H, *Fc*); -1.12 (s, br, 4H, *Fc*).

^{31}P {^{1}H} NMR ($CDCl_3$, 298 K, δ): 25.2.

2.4.5 Synthesis of Ln(BrMA)$_3${Fc(PPh$_2$O)$_2$} (Ln = Y, Eu, Yb; BrMA = conjugate base of bromomalonaldehyde)

For the synthesis of the bromomalonaldehyde complexes the same method of the nitromalonaldehyde was followed, dissolving 0.75 mmol (130 mg) of sodium bromomalonaldehyde in water instead of sodium nitromalonaldehyde. Yield: 57~61%

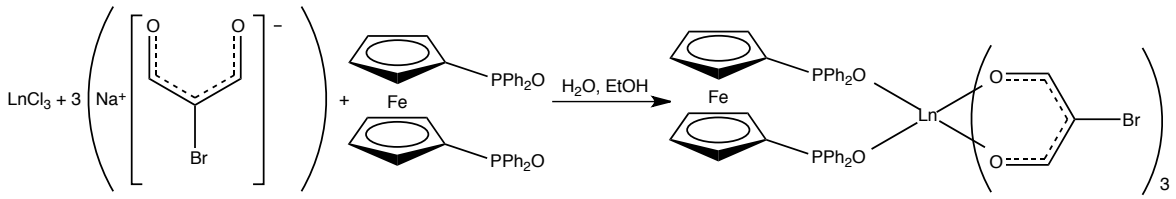

Scheme 2.13: Synthesis of Ln(BrMA)$_3${Fc(PPh$_2$O)$_2$}.

Characterization of Y(BrMA)$_3${Fc(PPh$_2$O)$_2$}

Elemental analysis: theoretical: C= 45.90%, H= 3.05%; found: C= 45.41%, H= 3.16%.

IR (KBr): 1560 cm^{-1} $\nu_{(CO)}$, 1152 cm^{-1} $\nu_{(P=O)}$.

^{1}H NMR (DMSO-d_6, 298 K, δ): 8.77 (s, br, 3H, BrMA); 7.70 - 7.40 (m, 20H, *Ph*); 4.45 (s, 4H, *Fc*); 4.36 (s, br, 4H, *Fc*).

^{31}P {^{1}H} NMR (DMSO-d_6, 298 K, δ): 26.8 br

UV-vis (CH_2Cl_2, 298 K, nm): <365, max 229 (ε = 51250 M^{-1} cm^{-1}); max 273 (ε = 30150 M^{-1} cm^{-1}); max 450 (ε = 500 M^{-1} cm^{-1}).

Characterization Eu(BrMA)$_3${Fc(PPh$_2$O)$_2$}

IR (KBr): 1558 cm^{-1} $\nu_{(CO)}$, 1154 cm^{-1} $\nu_{(P=O)}$.

Characterization of Yb(BrMA)$_3${Fc(PPh$_2$O)$_2$}

IR (KBr): 1559 cm^{-1} $\nu_{(CO)}$, 1160 cm^{-1} $\nu_{(P=O)}$.

3 Results and discussion

3.1 Group 3 and lanthanide complexes with the ligand 1-ferrocenyl-1,3-butanedionate

The study concerning new Group 3 and lanthanide complexes with ligands containing the ferrocene moiety started with the preparation of the β-diketonate 1-ferrocenyl-1,3-butandionate, K[FcCOCHCOCH$_3$], isolated as potassium salt. Two approaches were initially considered, the first one based on the reaction between acetylferrocene, deprotonated *in situ* with potassium *tert*-butoxide, and ethyl acetate in THF. After quenching with water and subsequent reaction with a stoichiometric amount of K[O^{t}Bu], the salt K[FcCOCHCOCH$_3$] was collected with acceptable yield (Scheme 3.1). In another series of experiments, the reaction of the ethyl ester of ferrocenecarboxylic acid (FcCOOC$_2$H$_5$) with proper nucleophiles was studied. The conjugate base of acetone was initially considered, but such a species is poorly stable and no product was obtained. Attempts to use more stable nucleophiles, deprotonated acetophenone in particular, were however unsuccessful, this indicating a scarce reactivity of FcCOOC$_2$H$_5$ (Scheme 3.1). It is however to be highlighted that these studies allowed to optimize the synthesis of FcCOOC$_2$H$_5$ with respect to the literature. The known methods are based on acid-catalyzed Fischer-type esterification, but differently from what reported, attempts to use such a method afforded FcCOOC$_2$H$_5$ in very low yield[39]. The intermediate reaction of ferrocenecarboxylic acid with PCl$_5$ and the subsequent reaction with ethanol allowed the isolation of FcCOOC$_2$H$_5$ with yield three-four times higher (Scheme 3.1). Replacement of PCl$_5$ with SOCl$_2$ caused the decomposition of the reactant.

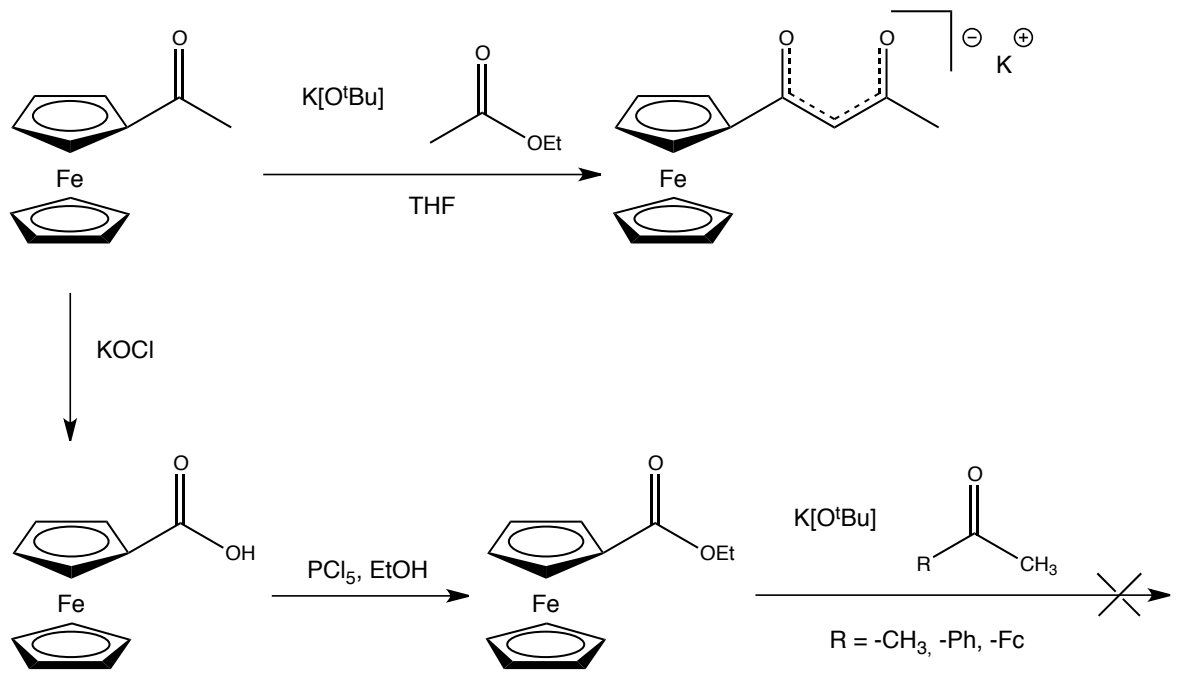

Scheme 3.1: Synthesis of ferrocene-based organic intermediates.

K[FcCOCHCOCH$_3$] was initially reacted with proper Group 3 and lanthanide anhydrous salts in THF in 3:1 stoichiometric ratio. Either $LnCl_3$ and $Ln(OTf)_3$ (OTf = triflate) precursors were employed, but these last gave products having general formula Ln(FcCOCHCOCH$_3$)$_3$ (Ln = Y, Eu, Yb) with higher yield and purity (Scheme 3.2).

Elemental analyses agree with the proposed formulae. The IR spectra are closely comparable, suggesting negligible variations of the coordination sphere on changing the metal centre, and show around between 1600 and 1500 cm^{-1} signals attributable to stretchings of the β-diketonate group (Figure 3.1).

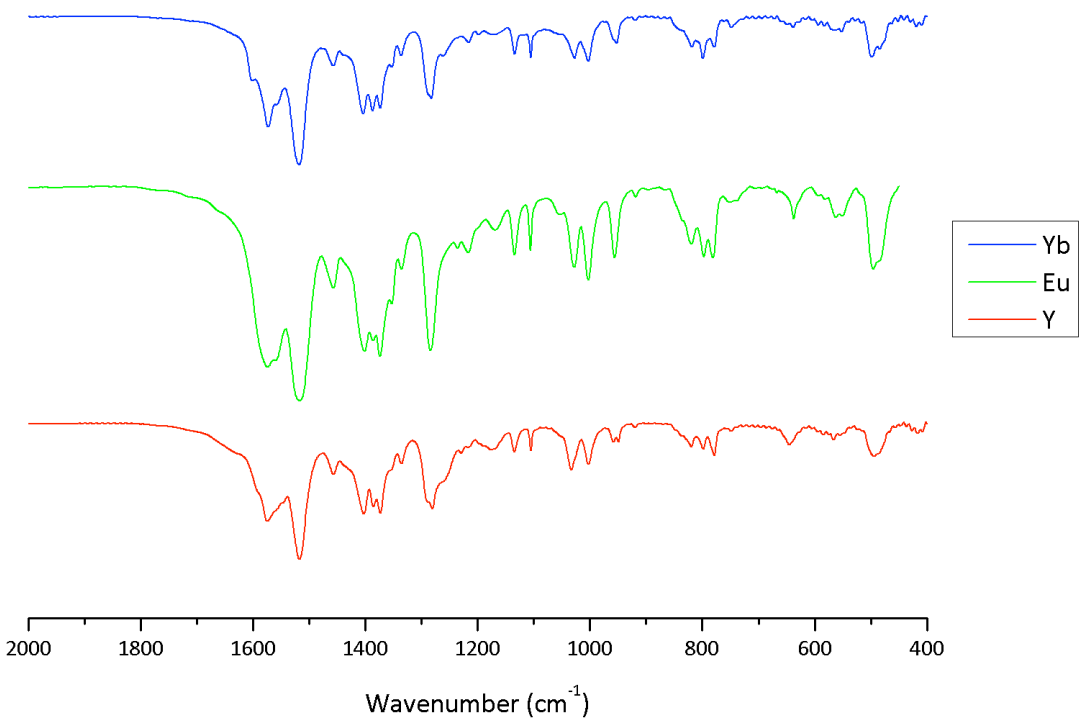

Figure 3.1: IR spectra of $Ln(FcCOCHCOCH_3)_3$ (Ln = Y, Eu, Yb).

The ^1H NMR spectrum of the diamagnetic yttrium derivative in deuterated dimethylsulfoxide shows three resonances attributable to the unsubstituted and substituted cyclopentadienyl rings in the range 4.8 - 4.1 ppm, one singlet for the central CH fragment at 5.77 ppm and a low-frequency singlet corresponding to the methyl group (Figure 3.2). The three ligands in the coordination sphere are therefore equivalent on the NMR timescale. It is worth noting that the resolution of the spectrum increased upon heating the sample at 338 K, probably because of the speed up of the fluxional processes that make the coordinated ligands equivalent. The formal replacement of Y^{3+} with paramagnetic centres causes shift and relaxation of the resonances[40]. For instance, in the ^1H NMR spectrum of $Eu(FcCOCHCOCH_3)_3$ reported in Figure 3.2 it is clearly observable the strong shift at lower frequencies of the CH and CH_3 resonances, while the ferrocenyl moiety appears comparatively less affected.

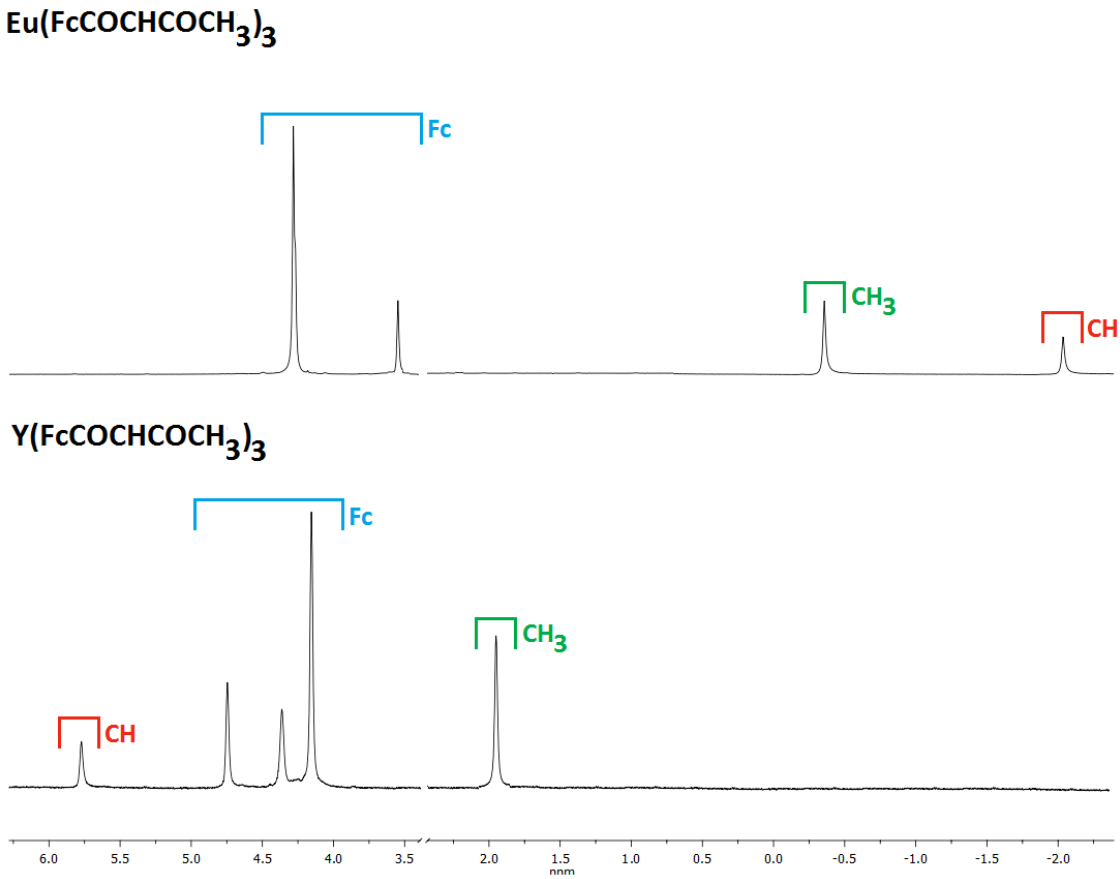

Figure 3.2: ^{1}H NMR spectra of Y(FcCOCHCOCH$_3$)$_3$ and Eu(FcCOCHCOCH$_3$)$_3$ in DMSO-d$_6$.

The ^{1}H NMR spectra above reported do not show any resonance attributable to coordinated THF. Lanthanide β-diketonate complexes having general formula Ln(β-dike)$_3$ are coordinatively unsaturated and mononuclear derivatives are usually observed only for centres with small ionic radius and bulky ligands in the coordination sphere, such as Lu(^{t}BuCOCHCO^{t}Bu)$_3$[41]. In most of the cases, β-diketonates behave as chelating-bridging ligands with the formation of oligomers. Unfortunately, we were unable to collect crystals suitable for X-ray diffractions, but joint electrochemical/diffusion experiments indicated for Y(FcCOCHCOCH$_3$)$_3$ a mononuclear structure in acetonitrile solution. A typical cyclic voltammogram at 50 mV/s scan speed is shown in Figure 3.3. Voltammograms collected at different scan speeds (10, 20 and 100 mV/s) are superimposable to that reported in Figure 3.3. The forward pick and the backward one result narrow, a good index of reversibility of the redox systems. The $E_{1/2}$ potential, 0.72 V vs. Ag/AgCl, is about 160 mV higher than that of ferrocene under the same experimental conditions, but this result can be easily justified by

the presence of an electron-withdrawing substituent on one of the cyclopentadienyl rings of $[FcCOCHCOCH_3]^-$ [42]. The quite oxidant behaviour of the corresponding ferricinium-based ligands prevented the formation of stable complexes by chemical oxidation. The diffusion coefficient of $Y(FcCOCHCOCH_3)_3$ was calculated on the basis of the stationary state Cottrell equation (time independent), typical for the disc-shape microelectrodes: $i = 4nFDCr$, where: i is the pick current (in A); n is the number of electrons exchanged during the redox process; F is the Faraday constant (96500 C mol^{-1}); D id the diffusion coefficient (in $cm^2\ s^{-1}$); C is the concentration (in mol cm^{-3}); r is the radius of the micro-electrode ($1.25\cdot10^{-3}$ cm)[43]. On assuming that each iron centre of $Y(FcCOCHCOCH_3)_3$ exchanges one electron, n = 3 and the diffusion coefficient is $1.9\cdot10^{-6}$ $cm^2\ s^{-1}$. Such a value is in good agreement with DOSY (diffusion ordered spectroscopy) NMR measurements on 10^{-3} M CD_3CN solutions of the complex.

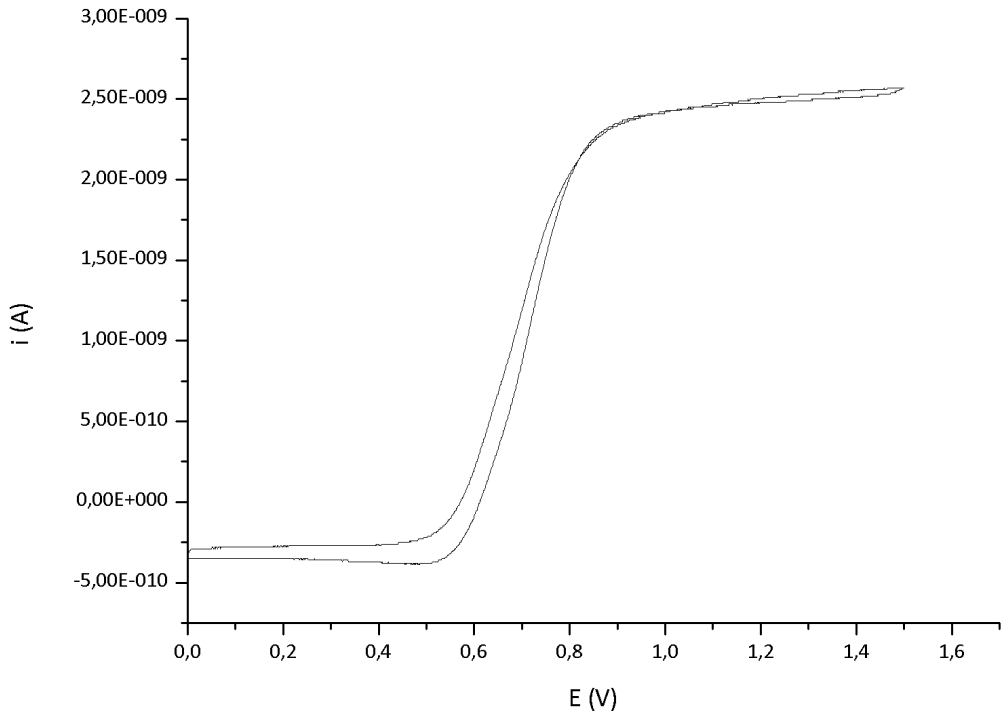

Figure 3.3: Cyclic voltammogram of $Y(FcCOCHCOCH_3)_3$ (10^{-3} M acetonitrile solution, platinum working microelectrode, scan speed 50 mV s^{-1}). Potentials are referred to the Ag/AgCl couple.

The complexes $Ln(FcCOCHCOCH_3)_3$ show the strongest absorptions in the UV range, even if a relatively weak band centred around 462 nm is present (see for example Figure 3.4). This absorption is usually attributed to the transition from the non-degenerate metal-centred

HOMO of ferrocene and the doubly-degenerate antibonding LUMO, where the participation of ligand orbitals is meaningfully higher[44].

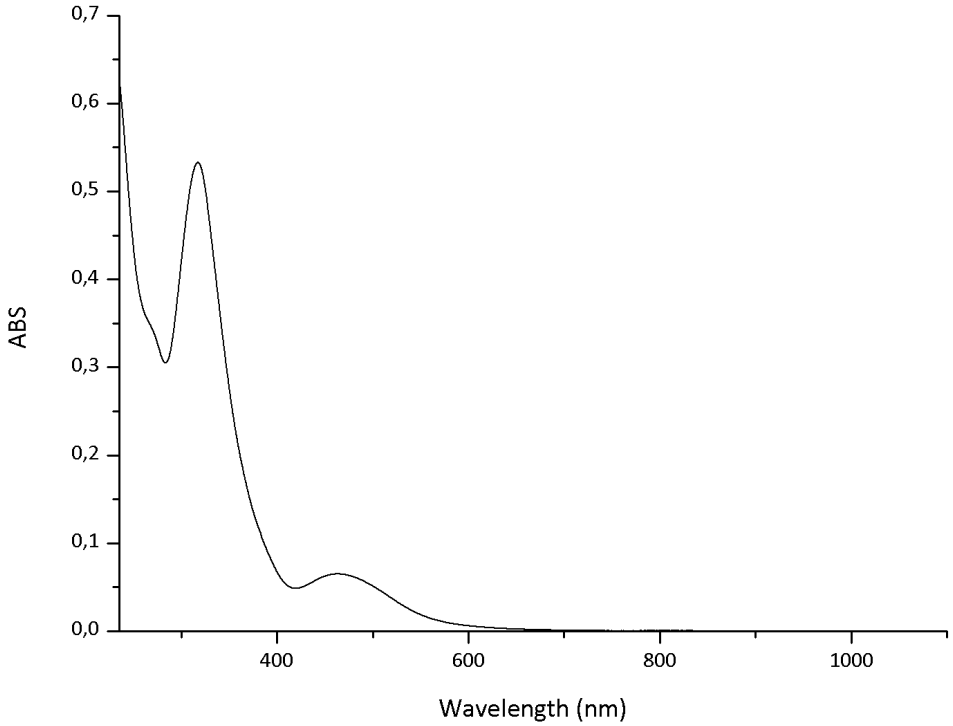

Figure 3.4: Absorption spectrum of $Y(FcCOCHCOCH_3)_3$ ($2.5 \cdot 10^{-5}$ M dichloromethane solution).

The photoluminescence of solid samples of the europium and ytterbium derivatives upon excitation with UV light was unfortunately too low to be detected. The lack of photoluminescence of $Eu(FcCOCHCOCH_3)_3$ is not surprisingly, on considering the possibility of back energy transfer from the $^5D_0$ resonance level of Eu^{3+} (ca. 17200 cm^{-1})[45] to lower energy states of the coordinated ligands. In fact, the first triplet state of pure ferrocene is estimated around 15000±1000 cm^{-1} [46]. On the other hand, the energy of the excited state of Yb^{3+} ($^2F_{5/2}$, ca. 10200 cm^{-1})[45] is low if compared to the ferrocene triplet state, so ytterbium-to-ferrocene energy transfer should be not possible. It is however to be highlighted that ferrocene is able to behave as quencher also towards luminescent organic compounds having triplet state below 13000 cm^{-1}, and in that case charge transfer mechanisms were invoked[46b]. DFT calculations carried out on the model system $YF_2(FcCOCHCOCH_3)$ gave the quintet state of this species about 24 kcal mol^{-1} higher than the corresponding singlet ground state. Moreover, the variations of the equilibrium geometry on changing the

multiplicity are quite scarce (root-mean-square deviation = 0.38 Å, see Figure 3.5). This energy gap is lower than that saturated by the $^2F_{5/2} \rightarrow {}^2F_{7/2}$ transition of Yb^{3+} (about 29 kcal mol^{-1}). It is therefore likely to suppose that a possible quenching pathway could involve the high-spin state of the ferrocene-based ligand.

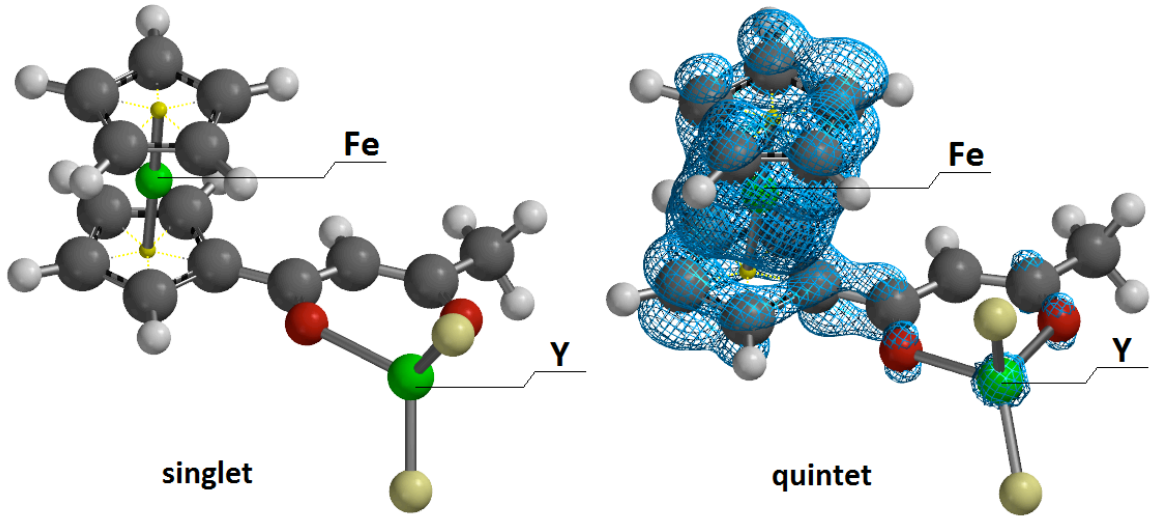

Figure 3.5: DFT-optimized structure of $YF_2(FcCOCHCOCH_3)$ in singlet and quintet state and spin density surface (isovalue = 0.001 a.u.).

These preliminary results are in agreement with the negligible luminescence already observed during previous studies on europium and ytterbium ferrocenecarboxylates[47].

Attempts to enhance the photoluminescence of lanthanide complexes containing the ferrocenyl-based β-diketonate where carried out by synthesizing heteroleptic complexes having N-donor ligands in their coordination sphere. 1,10-phenanthroline (phen) was chosen because of its widespread use in luminescent β-diketonate lanthanide complexes[48]. The tridentate ligand tris(3,5-dimethylpyrazol-1-yl)borate (Tp^{Me2}) was selected because of the antenna-effect shown by this type of scorpionates towards visible- and NIR-emitting lanthanide ions[49] and because of the ease of formation of heteroleptic complexes with anionic O-donor ligands[50].

Complexes having formulae $Ln(FcCOCHCOCH_3)_3(phen)$ (Ln = Y, Eu, Yb) where obtained by reacting the corresponding tris(β-diketonates) with one equivalent of 1,10-phenanthroline in dichloromethane at room temperature (Scheme 3.2). The synthesis of

$Ln(FcCOCHCOCH_3)(Tp^{Me2})_2$ (Ln = Y, Eu, Yb) required the *in situ* formation of the intermediates $Ln(OTf)(Tp^{Me2})_2$ from $Ln(OTf)_3$ and $K[Tp^{Me2}]$ and the subsequent reaction with one equivalent of $K[FcCOCHCOCH_3]$ in THF (Scheme 3.2).

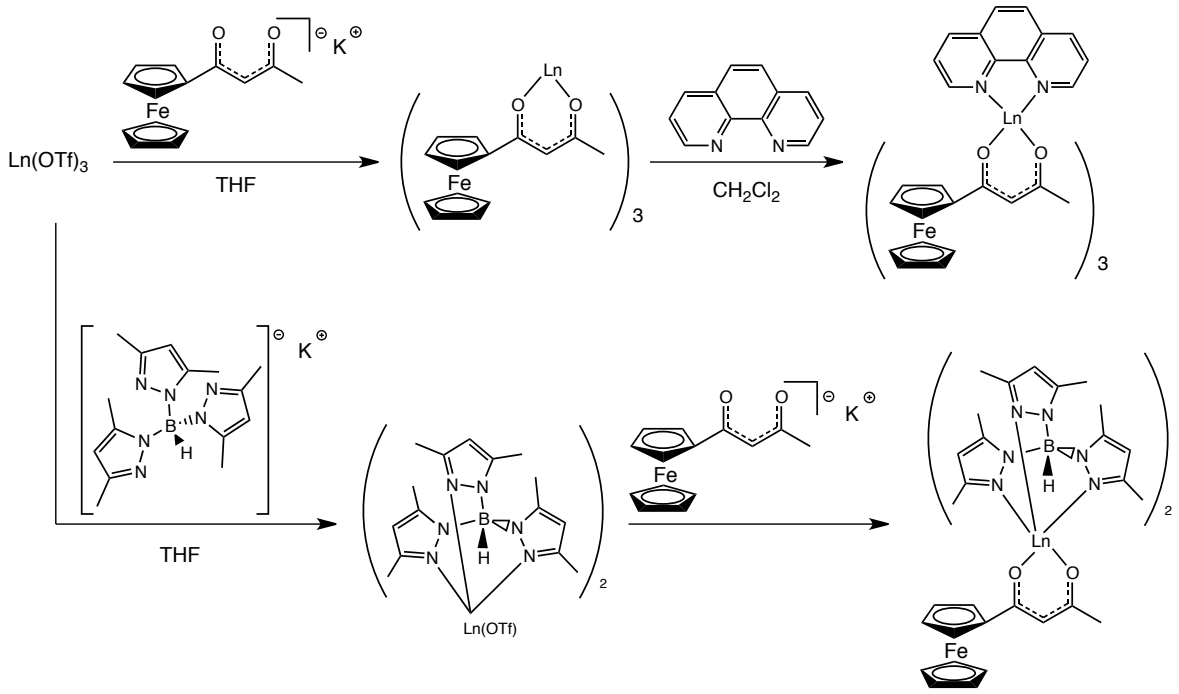

Scheme 3.2: Synthesis of yttrium and lanthanide heteroleptic complexes containing the ligand 1-ferrocenyl-1,3-butandionate.

Elemental analyses are in agreement with the proposed formulations. The typical stretchings of the β-diketonate moieties are clearly observable in the vibrational spectra of $Ln(FcCOCHCOCH_3)_3(phen)$ (Figure 3.6) and $Ln(FcCOCHCOCH_3)(Tp^{Me2})_2$ (Figure 3.7). The IR spectra of these last species also show a relatively weak band around 2550 cm^{-1} attributable to the B-H stretchings of the scorpionate ligands.

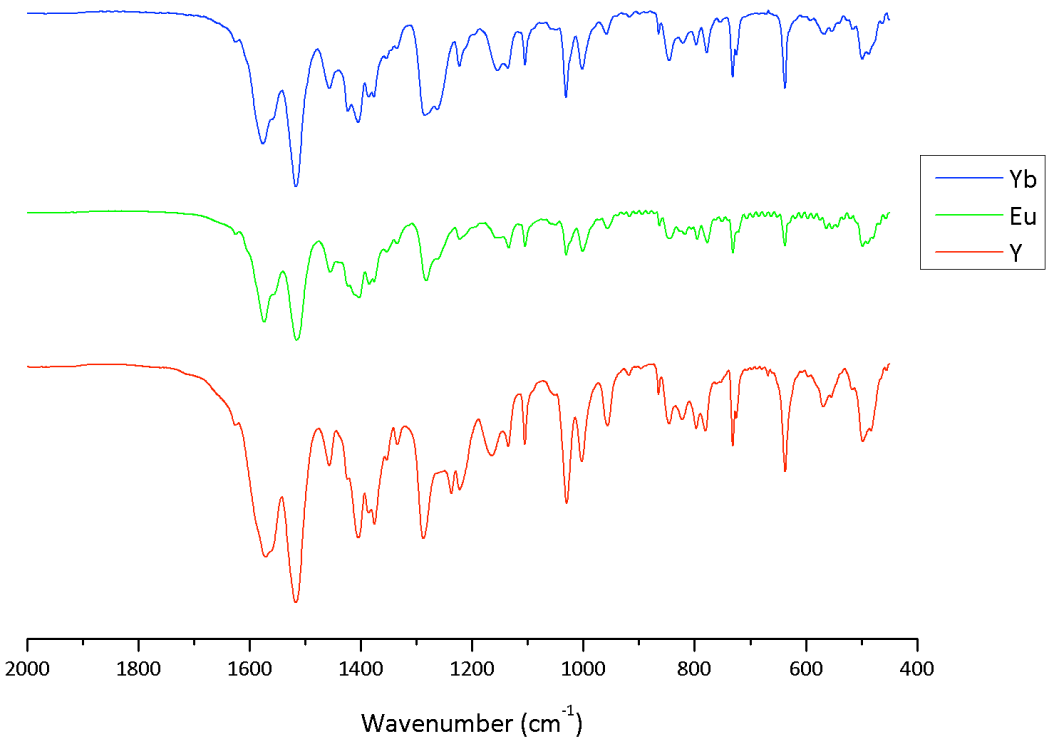

Figure 3.6: IR spectra of Ln(FcCOCHCOCH$_3$)$_3$(phen) (Ln = Y, Eu, Yb).

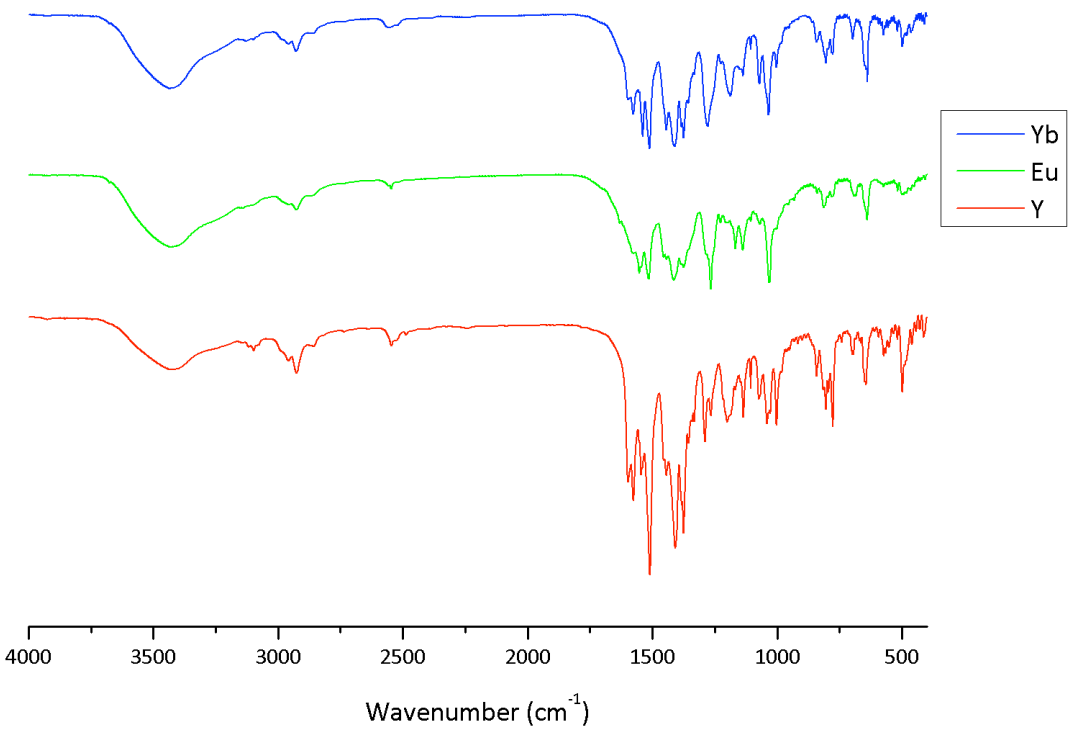

Figure 3.7: IR spectra of Ln(FcCOCHCOCH$_3$)(Tp^{Me2})$_2$ (Ln = Y, Eu, Yb).

The presence of the coordinated N-donor ligands besides the β-diketonates was confirmed by the ^{1}H NMR spectra, those of the diamagnetic yttrium derivatives in particular. In the ^{1}H NMR spectrum of Y(FcCOCHCOCH$_3$)$_3$(phen) (Figure 3.8) four high-frequency broad singlets attributable to 1,10-phenanthroline are present. The CH and CH$_3$ resonances of the β-diketonate ligands have chemical shift values comparable to those of the precursor. The cyclopentadyenyl signals in the range 4.90 - 3.85 ppm are quite broad and confused. This result and the broadness of the N-donor resonances suggest that the crowding in the yttrium coordination sphere slows the ferrocenyl rotations and the fluxional behaviour. Heating the sample leads to the progressive sharpening of the signals. In the case of the scorpionate derivative Y(FcCOCHCOCH$_3$)$_2$(Tp^{Me2})$_2$, the preliminary ^{1}H NMR spectrum recorded at 298 K was quite confused and composed by several resonances because of the non-equivalence of the pyrazole rings. Heating the sample caused the partial displacement of the N-donor ligands by dimethylsulfoxide, which behaves as O-donor ligand towards Group 3 and lanthanide trivalent ions[51]. The spectrum collected after heating, reported in Figure 3.9, is composed by one set of resonances for Tp^{Me2} and one for the β-diketonate ligand.

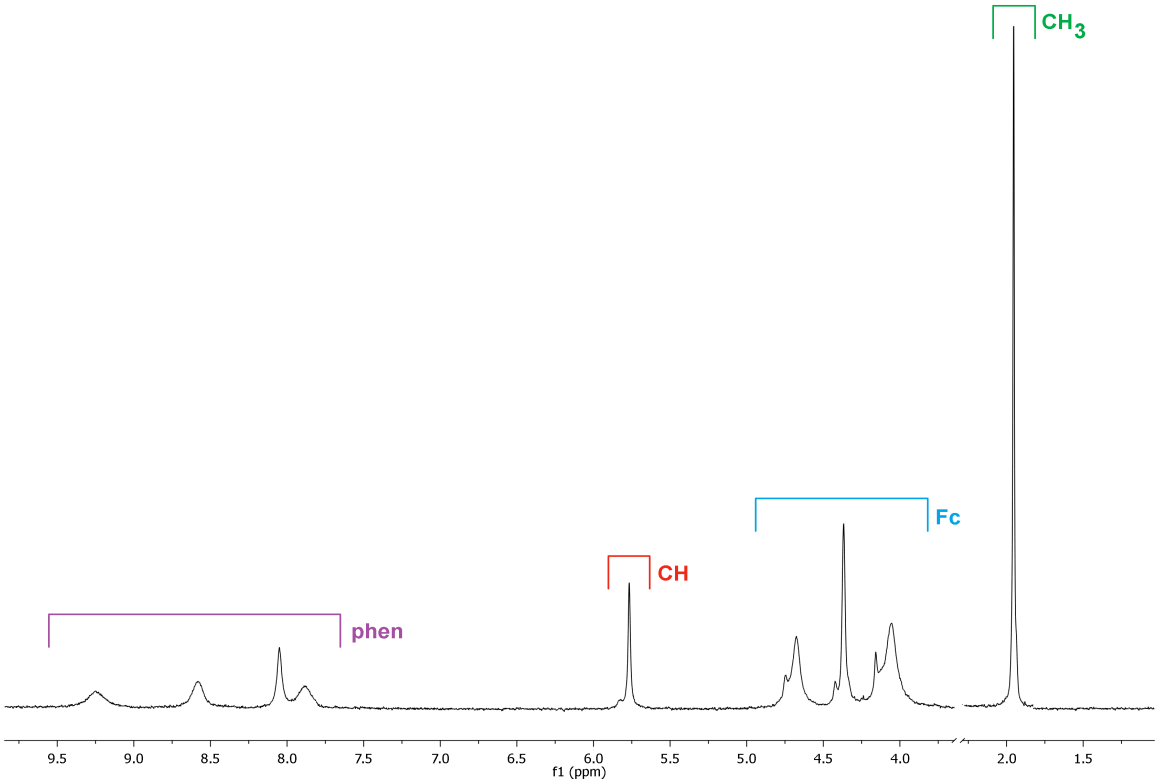

Figure 3.8: ^{1}H NMR spectrum of Y(FcCOCHCOCH$_3$)$_3$(phen) (DMSO-d$_6$, 298 K).

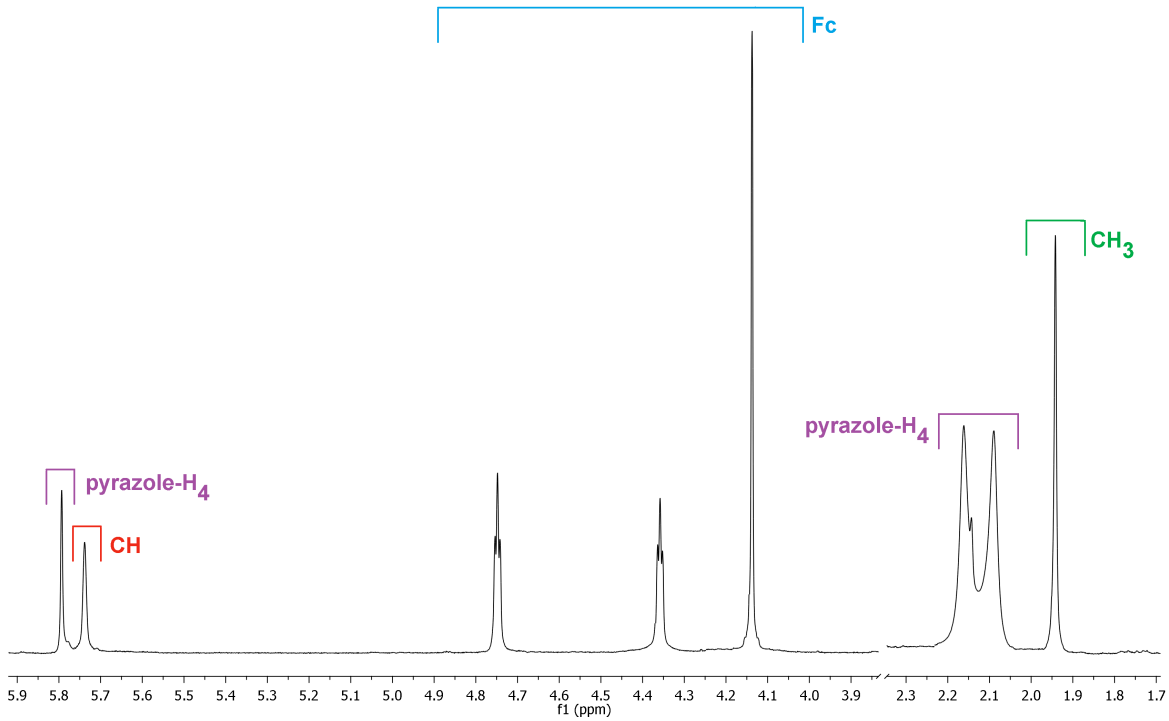

Figure 3.9: ^{1}H NMR spectrum of Y(FcCOCHCOCH$_3$)$_2$(Tp^{Me2})$_2$ (DMSO-d$_6$, 298 K) after heating the sample at 350 K.

Electrochemical measurements on Y(FcCOCHCOCH$_3$)$_2$(phen) and Y(FcCOCHCOCH$_3$)(Tp^{Me2})$_2$ showed quite reversible redox processes for the ferrocenyl moieties, comparable to that previously described for Y(FcCOCHCOCH$_3$)$_3$ (see Figure 3.10). The $E_{1/2}$ potentials indicate a small reduction of the oxidation potential for the heteroleptic complexes with respect to Y(FcCOCHCOCH$_3$)$_3$ (0.72 V), being 0.69 V and 0.62 V respectively for the phen and Tp^{Me2} derivative. The diffusion coefficients of Y(FcCOCHCOCH$_3$)(Tp^{Me2})$_2$ derived from the cyclic voltammogram, $1.1 \cdot 10^{-5}$ cm^2 s^{-1}, is in good agreement with that obtained from NMR DOSY measurements (inset of Figure 3.10).

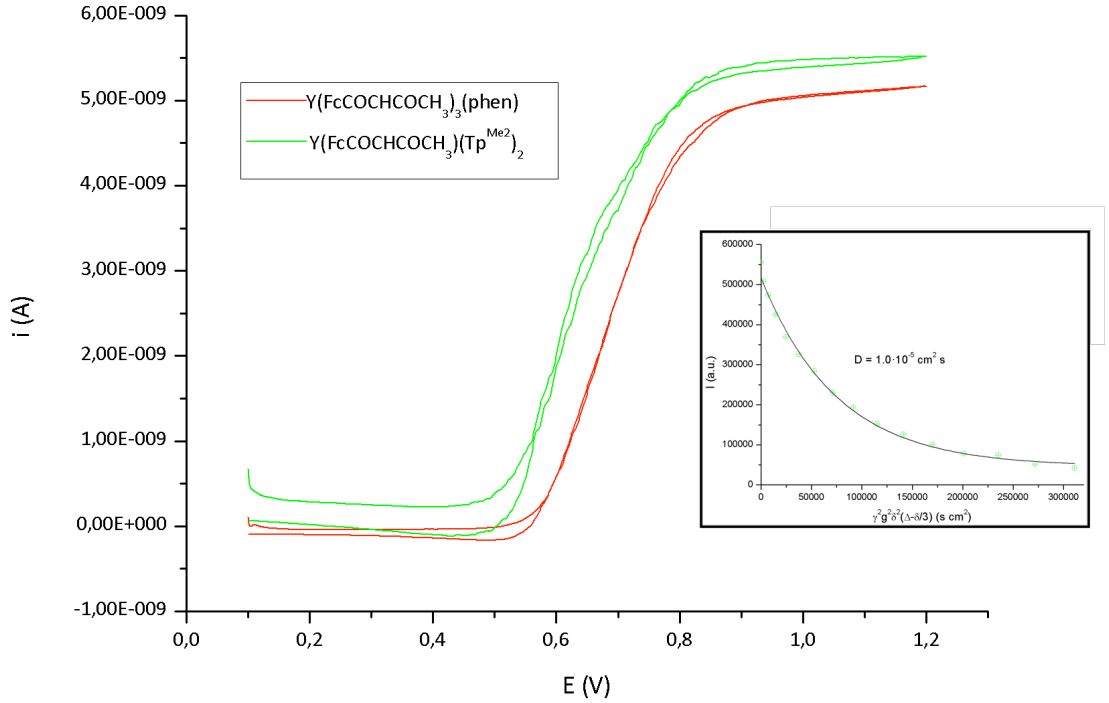

Figure 3.10: Cyclic voltammograms of $Y(FcCOCHCOCH_3)_3(phen)$ (red curve) and $Y(FcCOCHCOCH_3)(Tp^{Me2})_2$ (10^{-3} M acetonitrile solution, platinum working microelectrode, scan speed 50 mV s^{-1}). Potentials are referred to the Ag/AgCl couple. Inset: exponential fit of DOSY measurement on $Y(FcCOCHCOCH_3)(Tp^{Me2})_2$ in CD_3CN.

The UV-vis spectra of the heteroleptic complexes are closely comparable to those of the precursors $Ln(FcCOCHCOCH_3)_3$, being dominated by the absorptions of the ferrocenyl-β-diketonate ligands. The presence of 1,10-phenanthroline in the spectrum of $Y(FcCOCHCOCH_3)_3(phen)$ is evidenced by a strong band centred at 265 nm (Figure 3.11). Coordinated pyrazole-based scorpionates are more difficult to detect in the spectrum of $Y(FcCOCHCOCH_3)_2(Tp^{Me2})_2$, because this type of ligands is usually characterized by relatively weak absorptions for wavelengths below 300 nm[49].

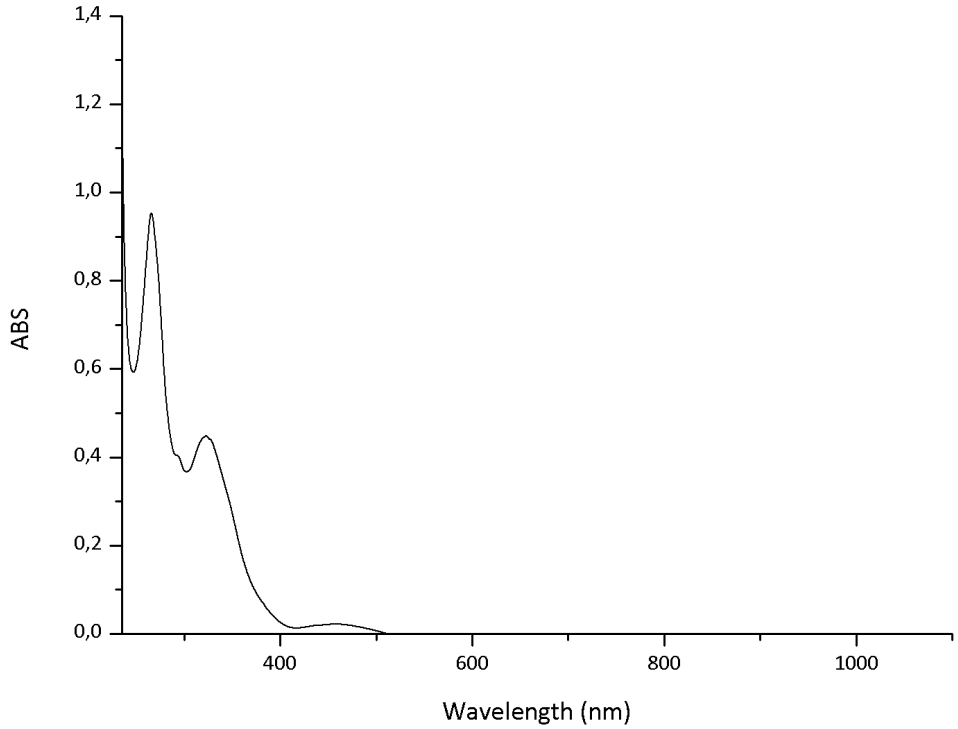

Figure 3.11: Absorption spectrum of $Y(FcCOCHCOCH_3)_3(phen)$ ($2.5 \cdot 10^{-5}$ M dichloromethane solution).

The changes in the coordination sphere of the complexes caused by the introduction of N-donor ligands did not cause any appreciable improvement of the photoluminescence of the europium and ytterbium derivatives, which resulted completely quenched by the ferrocenyl-β-diketonate. This influence is easily observable from the comparison of the emission spectrum of $Eu(FcCOCHCOCH_3)(Tp^{Me2})_2$ with that of the luminescent crude precursor $Eu(OTf)(Tp^{Me2})_2$, reported in Figure 3.12.

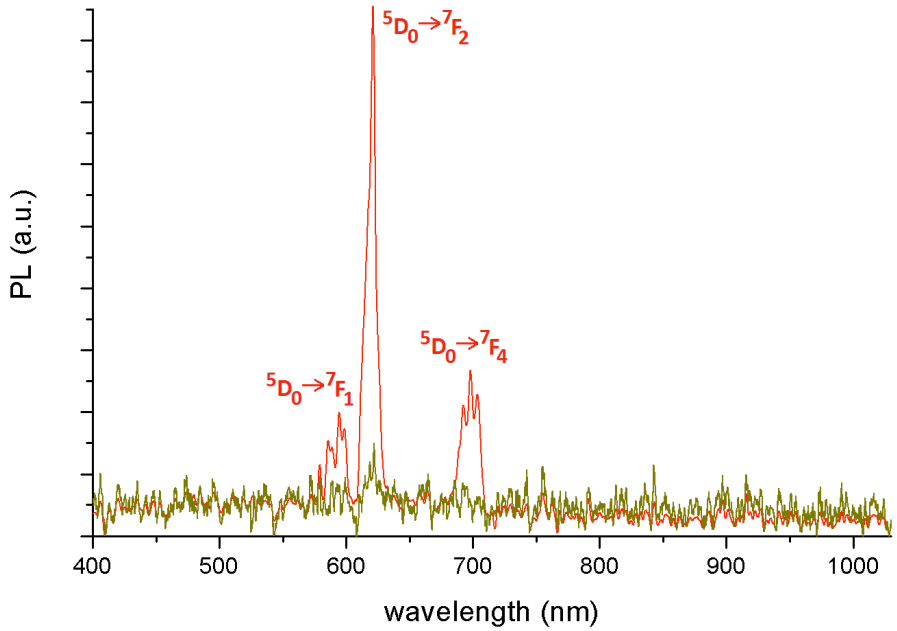

Figure 3.12: Emission spectra of Eu(FcCOCHCOCH$_3$)(Tp^{Me2})$_2$ (dark yellow line) and Eu(OTf)(Tp^{Me2})$_2$ (red line). Solid samples, 298 K, $\lambda_{excitation}$ = 280 nm.

3.2 Group 3 and lanthanide complexes with the ligand 1,1'-bis(diphenylphosphino)ferrocene dioxide

Further attempts to obtain new luminescent lanthanide complexes having ferrocene-based ligands in their coordination sphere were carried out using the neutral O-donor ligand bis(diphenylphosphino)ferrocene dioxide, Fc(PPh$_2$O)$_2$, which was prepared by oxidizing with H_2O_2 the corresponding phosphine. This ligand was coordinated to Group 3 and lanthanide metal fragments of the type [Ln(O-O)$_3$], where O-O represents the conjugate base of a β-dialdehyde, nitromalonaldehyde (NMA) and bromomalonaldehyde (BrMA) in particular. These ancillary ligands were chosen because of the photoluminescence exhibited in the past by most of their lanthanide complexes, in particular in the visible range, and because of the possible formation of coordination compounds with ligands such as triphenylphosphine oxide[52]. Compounds having general formula Ln(O-O)$_3${Fc(PPh$_2$O)$_2$} (Ln = Y, Eu, Yb; O-O = NMA, BrMA) were obtained under mild conditions by subsequent reaction of LnCl$_3$ with the proper salt of the β-dialdehyde and the bis(phosphine oxide) in water/ethanol, as summarized in Scheme 3.3.

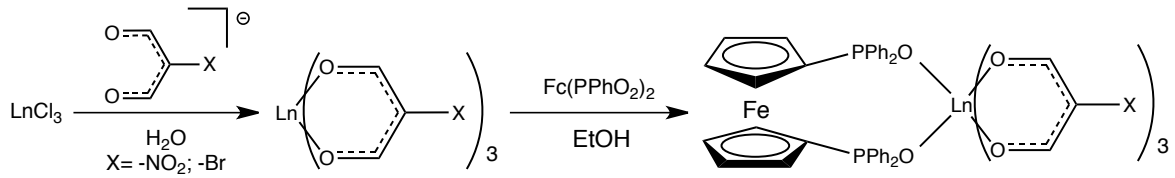

Scheme 3.3: Synthesis of $Ln(O\text{-}O)_3\{Fc(PPh_2O)_2\}$ (Ln = Y, Eu, Yb; O-O = NMA, BrMA).

Characterization data agree with the proposed formulations. The presence of the ligand $Fc(PPh_2O)_2$ is highlighted in the IR spectra by a medium intensity band around 1150 – 1160 cm^{-1} corresponding to P=O stretching (Figures 3.13 and 3.14). The NMA derivatives also show a strong signal around 1648 – 1650 cm^{-1} due to the conjugated carbonyl stretching. The asymmetric and symmetric stretchings of the nitro groups fall around 1507 and 1317 cm^{-1}, respectively. In the IR spectra of the BrMA complexes the stretching most involving the carbonyl fragments corresponds to a strong band at ca. 1559 cm^{-1}. As already observed for the complexes described in the previous chapter, the change of metal centre causes negligible variations in the IR spectra.

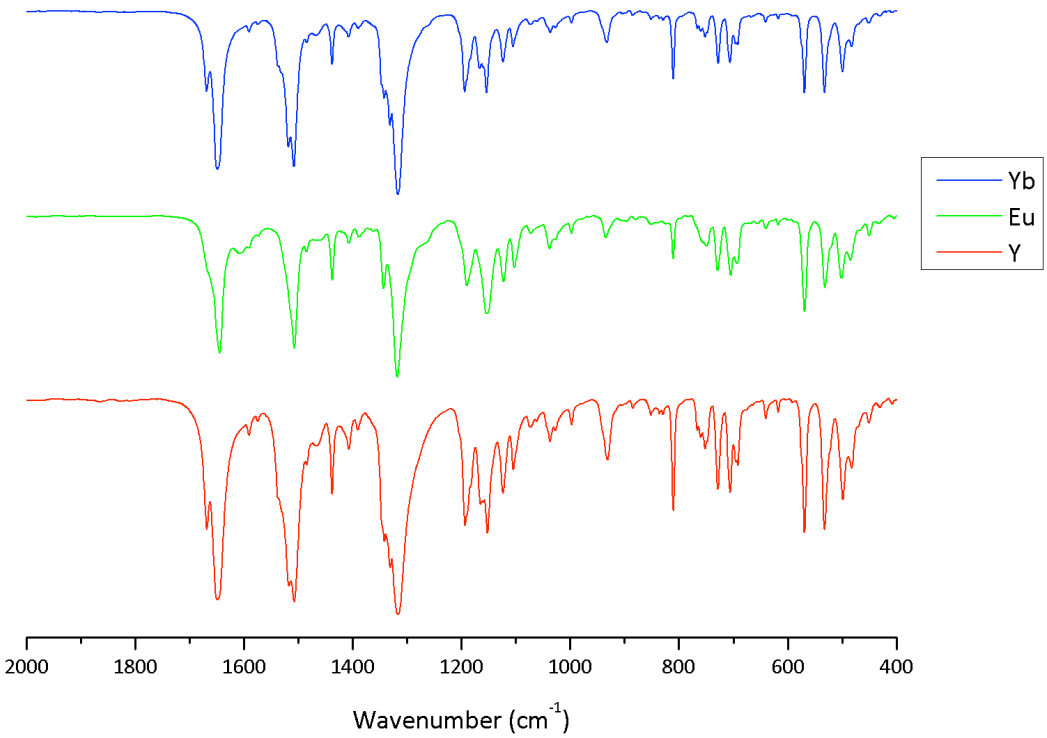

Figure 3.13: IR spectra of $Ln(NMA)_3\{Fc(PPh_2O)_2\}$ (Ln = Y, Eu, Yb).

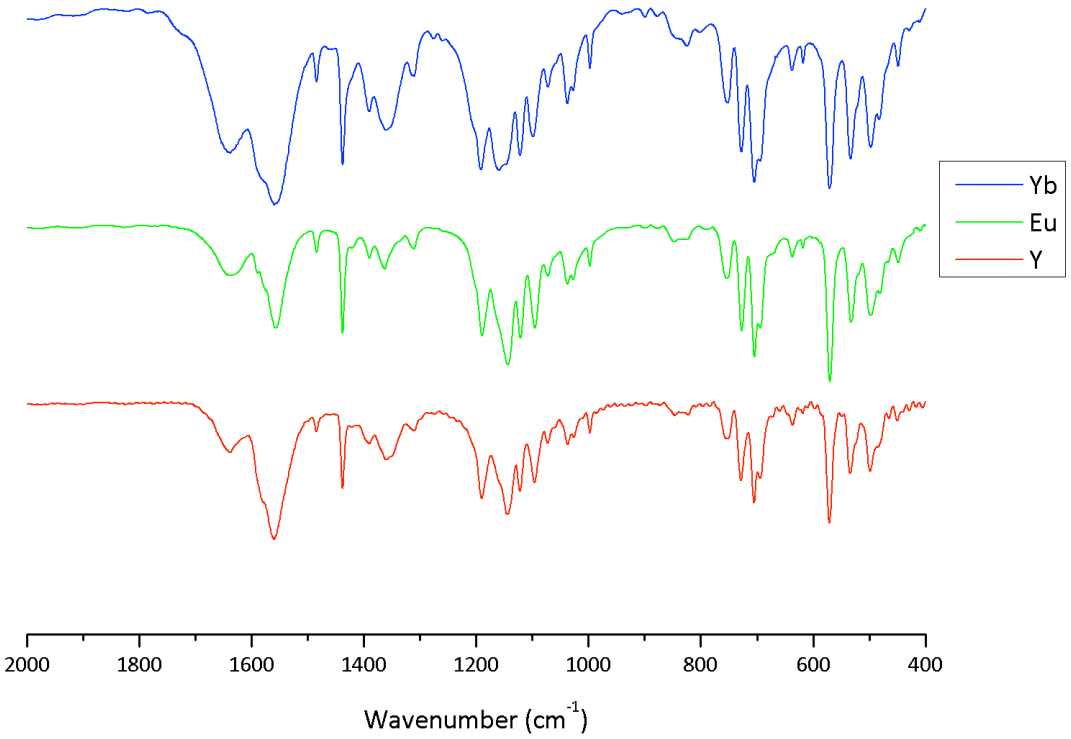

Figure 3.14: IR spectra of $Ln(BrMA)_3\{Fc(PPh_2O)_2\}$ (Ln = Y, Eu, Yb).

The ^1H NMR spectra in $CDCl_3$ show two signals for the non-equivalent protons of the substituted cyclopentadienyl rings, a set of resonances for the phenyl substituents and a singlet for the coordinated β-dialdehydes. Either the O-donor chelating ligands and the coordinating moieties of $Fc(PPh_2O)_2$ are therefore equivalent on the NMR timescale. The resonances are meaningfully affected by paramagnetic shift on changing the yttrium centre with europium or ytterbium, as observable for instance in Figure 3.15, which compares the ^1H NMR spectra of $Y(NMA)_3\{Fc(PPh_2O)_2\}$ and $Yb(NMA)_3\{Fc(PPh_2O)_2\}$. The $^{31}P\{^1H\}$ NMR spectra of NMA complexes show in all the cases only one signal, and the coupling between ^{31}P and ^{89}Y ($^2J_{P\text{-}Y}$ = 9.8 Hz) supports the coordination of the bis(phosphine oxide) (Figure 3.16). In the case of $Y(BrMA)_3\{Fc(PPh_2O)_2\}$ only a broad resonance was instead detected, probably because of fluxional behaviour.

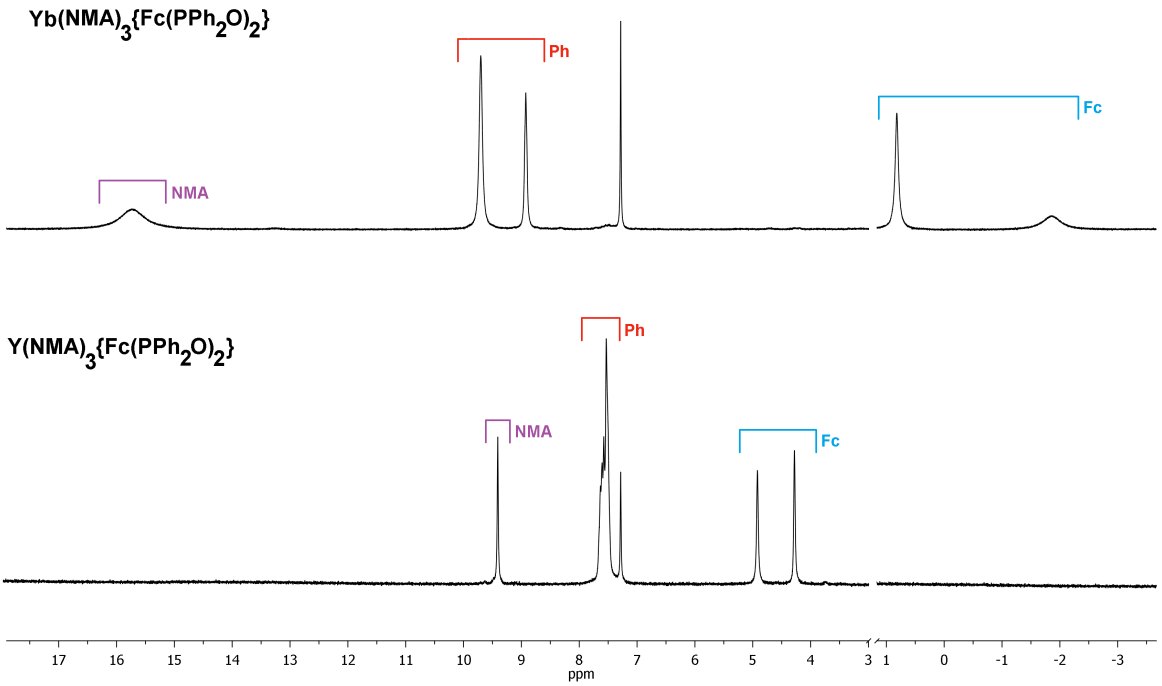

Figure 3.15: ^{1}H NMR spectra of $Y(NMA)_3\{Fc(PPh_2O)_2\}$ and $Yb(NMA)_3\{Fc(PPh_2O)_2\}$ ($CDCl_3$, 298 K).

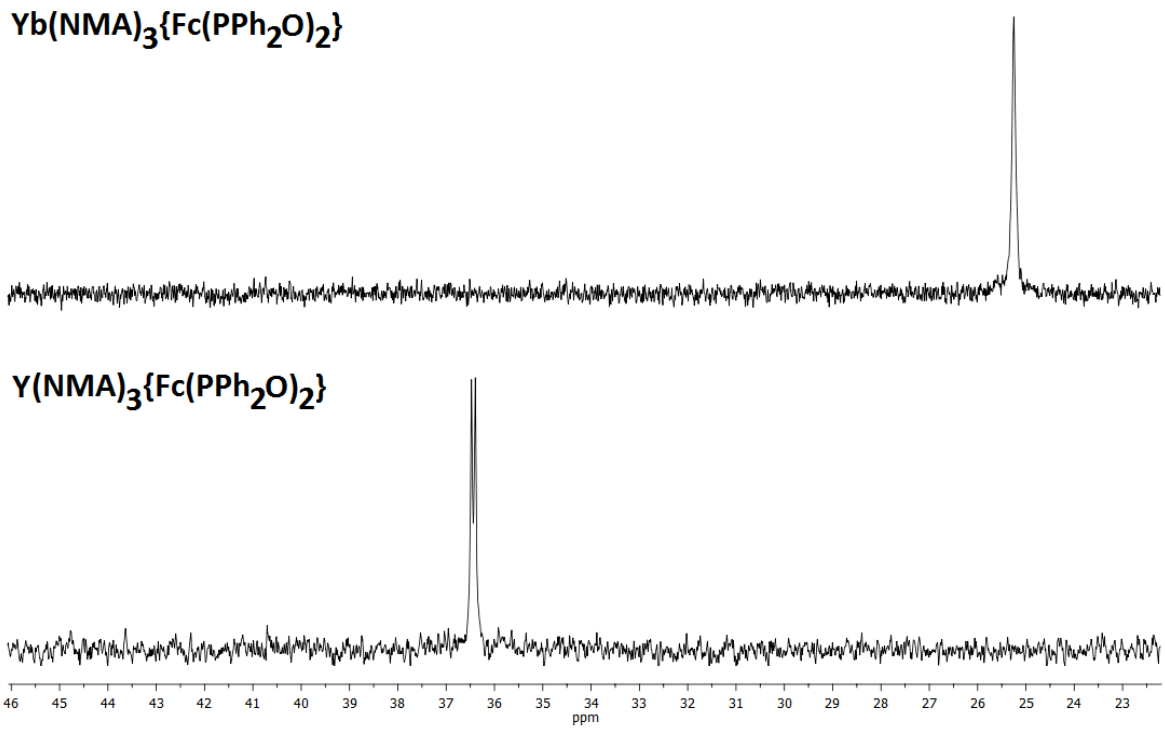

Figure 3.16: ^{31}P $\{^{1}H\}$ NMR spectra of $Y(NMA)_3\{Fc(PPh_2O)_2\}$ and $Yb(NMA)_3\{Fc(PPh_2O)_2\}$ ($CDCl_3$, 298 K).

Electrochemical measurements were carried out either on $Y(NMA)_3\{Fc(PPh_2O)_2\}$ and $Y(BrMA)_3\{Fc(PPh_2O)_2\}$, but preliminary experiments showed that the oxidation of this last compound involves not only the ferrocenyl-based phosphine oxide, but also the other ancillary ligands. The cyclic voltammogram of $Y(NMA)_3\{Fc(PPh_2O)_2\}$ is instead comparable to that of free $Fc(PPh_2O)_2$, even if the peak current is lower because of the minor diffusion coefficient. Quite interestingly, the coordination to the $[Y(NMA)_3]$ fragment causes the increase of the $E_{1/2}$ potential by about 0.1 V from the 1.03 V of $Fc(PPh_2O)_2$ to the 1.13 V of $Y(NMA)_3\{Fc(PPh_2O)_2\}$, this indicating a relative destabilization of the corresponding ferricinium derivative caused by coordination (see Figure 3.17 for the comparison of the cyclic voltammograms).

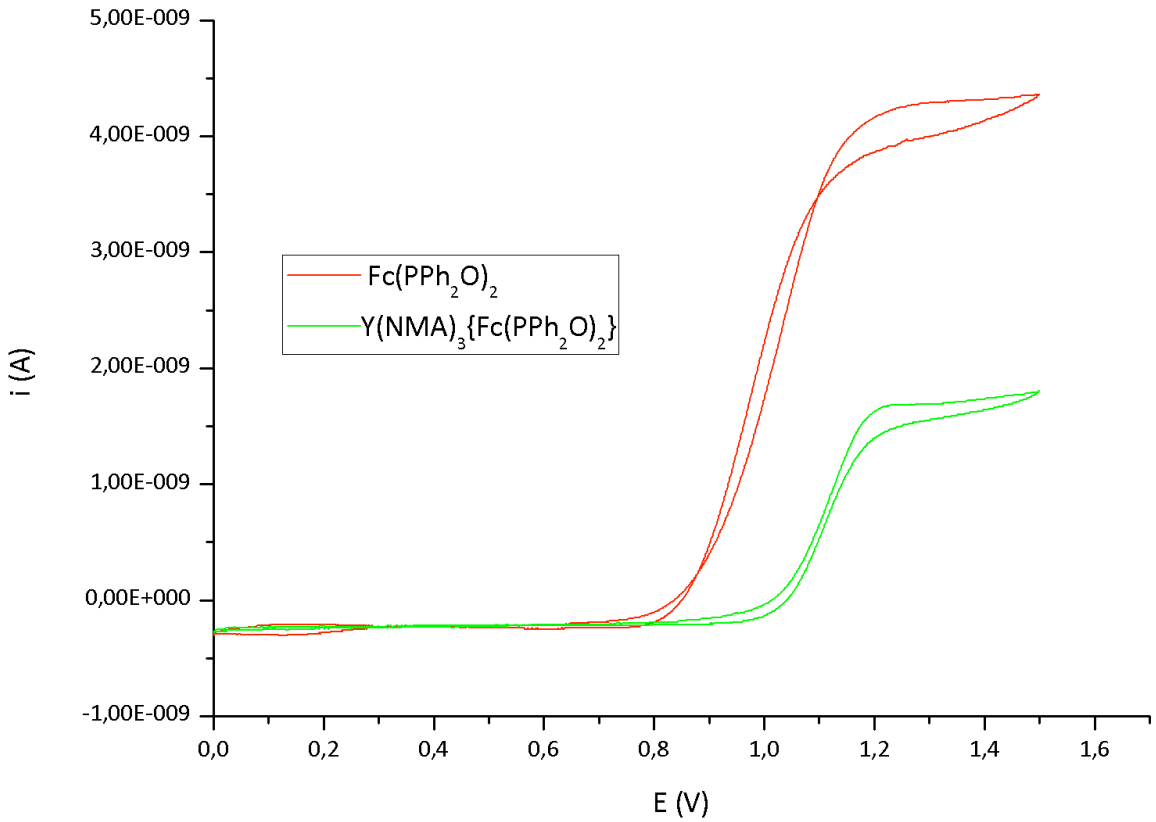

Figure 3.17: Cyclic voltammograms of the free ligand $Fc(PPh_2O)_2$ (red curve) and $Y(NMA)_3\{Fc(PPh_2O)_2\}$ (green curve). 10^{-3} M acetonitrile solution, platinum working microelectrode, scan speed 50 mV s^{-1}. Potentials are referred to the Ag/AgCl couple.

The absorption spectra of the NMA- and BrMA-derivates are characterized by a weak band around 440 nm attributable to the transition from the non-degenerate metal-centred HOMO

of the ferrocenyl moiety and the doubly-degenerate delocalized antibonding LUMO. The lower conjugation of this last MO in $Fc(PPh_2O)_2$ with respect to $[FcCOCHCOCH_3]^-$ could explain the lower absorption coefficient with respect to what reported in the previous chapter. The change of ancillary ligands mainly influences the near-UV region, because the delocalization associated to the $-NO_2$ substituent extends the absorptions of the β-dialdehydes close to 400 nm (see Figures 3.18 and 3.19).

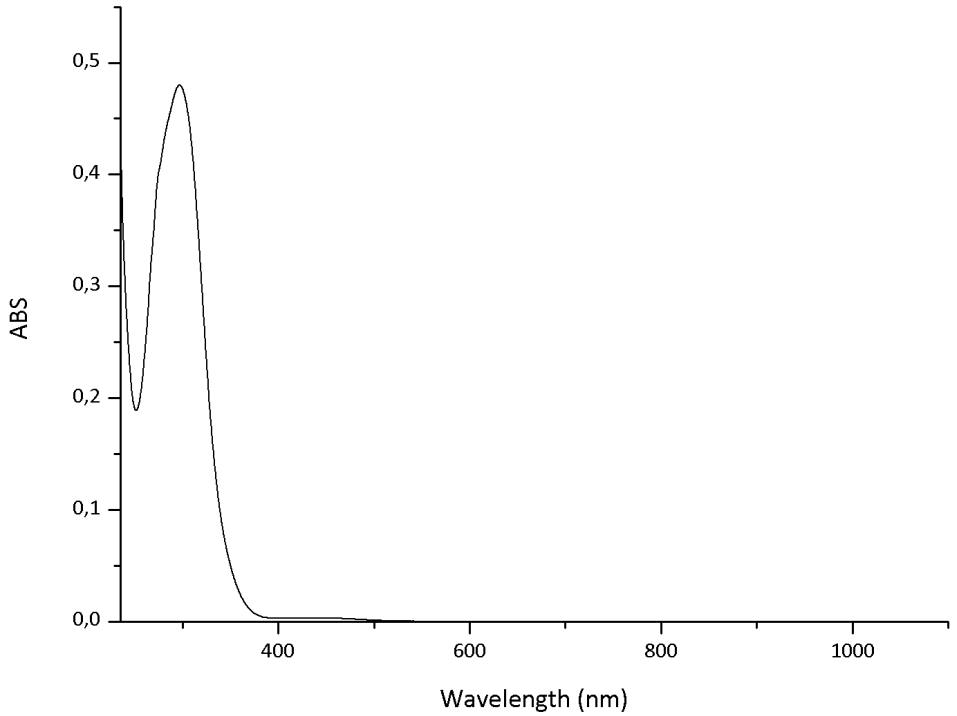

Figure 3.18: Absorption spectrum of $Y(NMA)_3\{Fc(PPh_2O)_2\}$ ($2.5\cdot10^{-5}$ M dichloromethane solution).

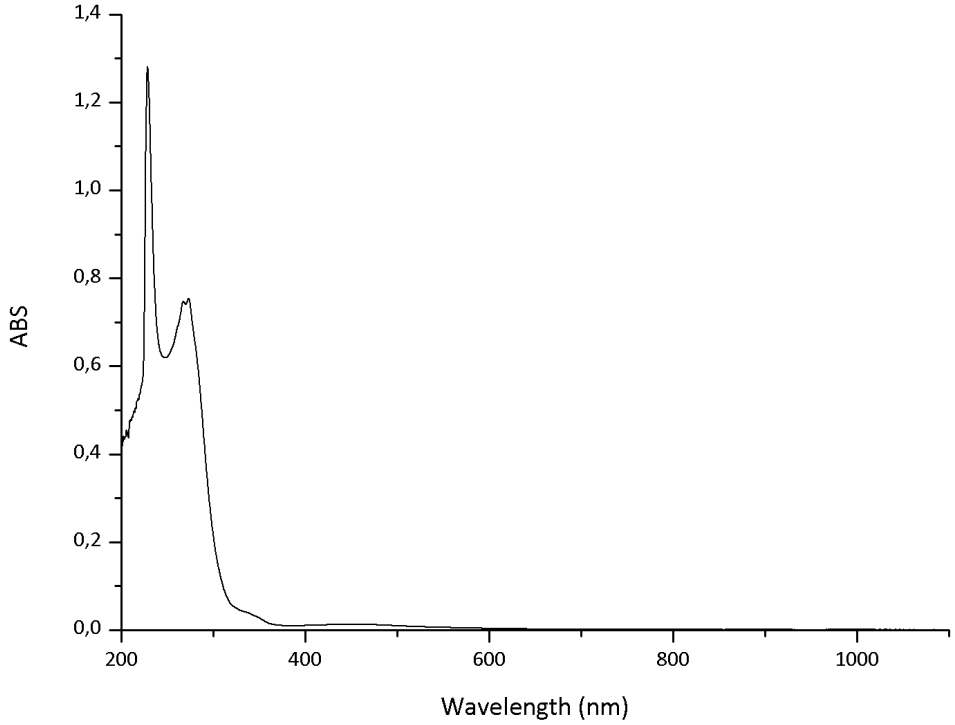

Figure 3.19: Absorption spectrum of $Y(BrMA)_3\{Fc(PPh_2O)_2\}$ ($2.5\cdot10^{-5}$ M dichloromethane solution).

Unfortunately, the luminescence quenching caused by the presence of the ferrocene fragment works efficiently also for the europium and ytterbium derivatives described in this chapter, despite the fact that the electronic structures of $Fc(PPh_2O)_2$ and $[FcCOCHCOCH_3]^-$ are completely different. As an example, Figure 3.20 compares the PL spectrum of $Eu(NMA)_3\{Fc(PPh_2O)_2\}$ with that of the crude reaction intermediate $Eu(NMA)_3(H_2O)_x$. The typical $^5D_0 \rightarrow {}^7F_J$ transitions of the Eu^{3+} ion are clearly observable in $Eu(NMA)_3(H_2O)_x$, superimposed to a ligand-based emission, while no signal was detected for $Eu(NMA)_3\{Fc(PPh_2O)_2\}$ under the same conditions.

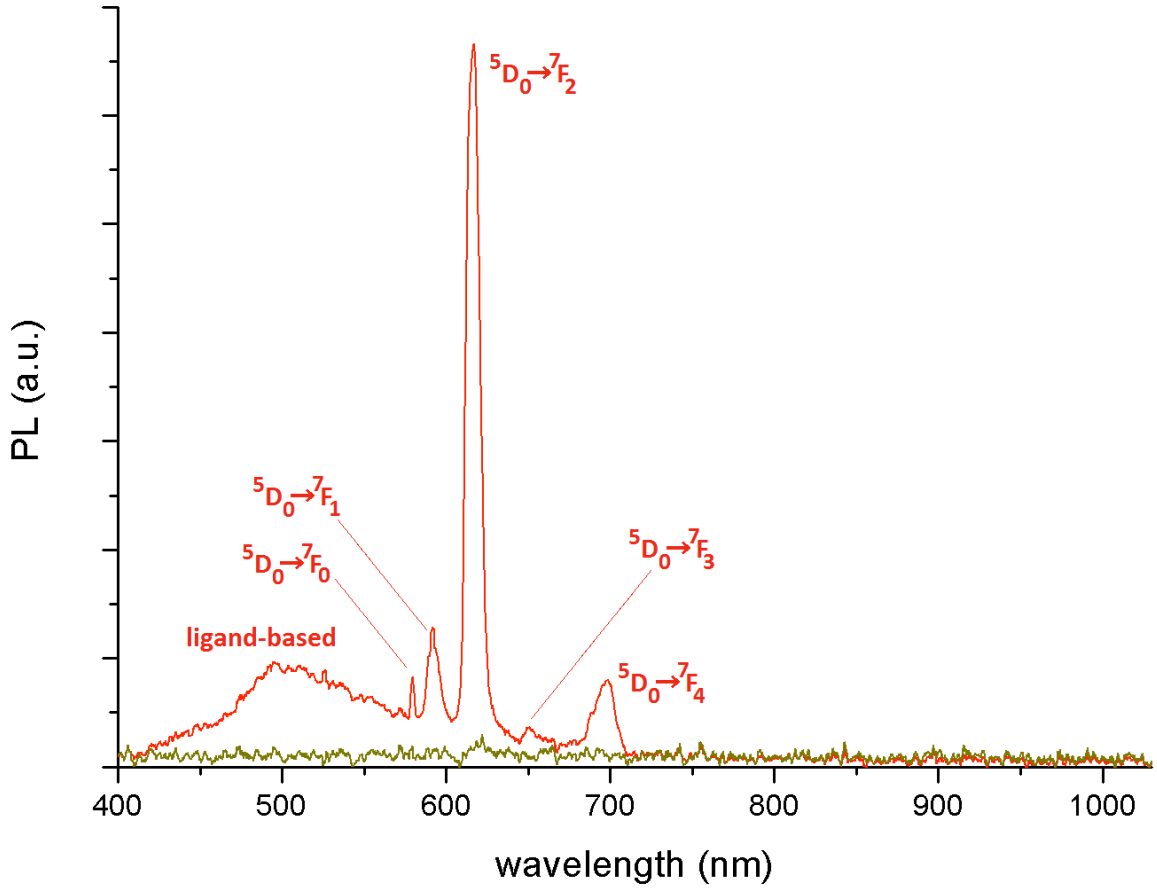

Figure 3.20: Emission spectra of $Eu(NMA)_3\{Fc(PPh_2O)_2\}$ (dark yellow line) and $Eu(NMA)_3(H_2O)_x$ (red line). Solid samples, 298 K, $\lambda_{excitation}$ = 375 nm.

4 Conclusions

This thesis reports the syntheses and characterizations of several Group 3 and lanthanide complexes with two different types of ferrocenyl-based O-donor ligands in their coordination sphere, based on the β-diketonate and phosphine oxide donor moieties. With the exception of the bromomalonaldehyde derivatives, the compounds undergo electrochemical processes comparable to that of ferrocene, even if the oxidation of the iron centre takes place at higher potentials. Despite their promising redox features, all the prepared derivatives of europium and ytterbium are not suited for joint luminescence/electrochemical applications. The ferrocenyl moiety completely quenches both the visible-emitting Eu^{3+} ion and the NIR-emitting Yb^{3+} ion, also in the presence of well-known antenna-ligands such as 1,10-phenantholine, tris(3,5-dimethyl-pyrazol-1-yl)borate, and the conjugate bases of nitromalonaldehyde and bromomalonaldehyde. This result is in agreement with previous outcomes concerning lanthanide ferrocenecarboxylates, studied by the research group where this thesis work has been developed. The lack of luminescence is also in agreement with papers reported in the past regarding the quench of organic luminescence by ferrocene. The presence in the recent literature of few luminescent ferrocene-containing europium complexes appears therefore an exceptional event, and detailed studies of the ligand-lanthanide energy transfer in these species should be carried out. Probably, one way to avoid the luminescence quenching is the increase of the intermetallic separation and the interruption of the electronic conjugation.

5 Bibliography

[1] O. Kahn, Molecular Magnetism, VCH, (1993).

[2] (a) R. H. Holm, P. Kennepohl, E. I. Solomon, Chem. Rev. 96 (1996) 2239; (b) S. Faulkner, J. L. Matthews, Comprehensive Coordination Chemistry, 2nded; M. D. Ward, Ed; Elsevier: Oxford, U.K., 9 (2004) 913 and internal references.

[3] N. Raymond, V. C. Pierre, M. Botta, S. Aime, N. Kenneth, J. Am. Chem. Soc. 128 (2006) 9272.

[4] P. Blaser, S. Bernhard, C. Blum, A. Beyeler, L. De Cola and V. Balzani, Coord. Chem. Rev. (1999) 190 and 155.

[5] Y. Wada, H. Nakashima, Y. Hasegawa, T. Ohkubo, K. Sogabe, S. Yanagida, Y. Kawamura, Angew. Chem. 112 (2000) 365.

[6] Y. Wada, K. Sogabe, S. Yanagida, Y. Hasegawa, J. Lumin. 101 (2003) 235 and references therein.

[7] (a) S. Faulkner, M. Tropiano, N. L. Kilah, M. Morten, H. Rahman, J. J. Davis, P. D. Beer, J. Am. Chem. Soc. 133 (2011) 11847; (b) S. Rigaut, E. Di Piazza, L. Norel. K. Costuas, A. Bourdolle, O. Maury, J. Am. Chem. Soc. 133 (2011) 6174.

[8] S. Cotton, Lanthanide and Actinide Chemistry, J. Wiley & Sons., Ltd, Rutland, UK, 2006.

[9] K. Binnemans, Chem. Rev. 109 (2009) 4283.

[10] H. Uh, S. Petoud, C. R. Chimie, 13 (2010) 668.

[11] M. D. Ward, N. M. Shavaleev, G. Accorsi, D. Virgili, Z. R. Bell, T. Lazarides, G. Calogero, N. Armaroli, Inorg. Chem. 44 (2005) 61.

[12] J. P. Sauvage, Molecular Machines & Motors. Structure & Bonding, Springer Verlag, 2001.

[13] (a) J. M. Herrera, S. J. A. Pope, A. J. H. M. Meijer, T. L. Easun, H. Adams, W. Z. Alsindi, X. Z. Sun, M. W. George, S. Faulkner, M. D. Ward, J. Am. Chem. Soc. 129 (2007) 11491; (b) T. Lazarides, G. M. Daviesa, H. Adams, C. Sabatini, F. Barigelletti, A. Barbieri, J. A. Pope, S. Faulkner, M. D. Ward, Photochem. Photobiol. Sci. (2007) 1152.

[14] (a) S. Kaizaki, M. A. Subhan, T. Sanada, T. Suzuky, J. Chem. Soc. Dalton Trans. (2001) 492; (b) S. Kaizaki, M. A. Subhan, T. Sanada, T. Suzuky, Inorg. Chim. Acta 353 (2003) 263.

[15] (a) M. D. Ward, N. M. Shavaleev, G. Accorsi, D. Virgili, Z. R. Bell, T. Lazarides, G. Calogero, N. Armaroli, Inorg. Chem. 44 (2005) 61; (b) M. D. Ward, S. Faulkner, D. Sykes, H. Adams, T. Lazarides, G. Calogero, Dalton Trans. (2008) 961.

[16] (a) F. Kennedy, N. M. Shavaleev, T. Koullourou,. Z. R. Bell, J. C. Jeffery, S. Faulkner, M. D. Ward, Dalton Trans. (2007) 1492; (b) N.M. Shavaleev, Z. R. Bell, M. D. Ward, J. Chem. Soc., Dalton Trans. (2002) 3925.

[17] S. Kaizaki, T. Tsukuda, T. Yagi, R. Kawahata, H. Nakata, A. Subhan, A. Fuyuhiro, Chem. Lett. 32 (2003) 1084.

[18] (a) D. Sykes, I. S. Tidmarsh, A. Barbieri, I. V. Sazanovich, J. A. Weinstein, M. D. Ward, Inorg. Chem. 50 (2011) 11323; (b) T. Lazarides, D. Sykes, S. Faulkner, A. Barbieri, M. D. Ward, Chem. Eur. J. 14 (2008) 9389.

[19] S.J. A. Pope, B. J. Coe, S.Faulkner, E. V. Bichenkova, X. Yu, K. T. Douglas, J. Am. Chem. Soc. 126 (2004) 9490.

[20] M. Tropiano, C. J. Record, E. Morris, H. S. Rai, C. Allain, S. Faulkner, Organometallics 31 (2012) 5673.

[21] S. Faulkner, A. M. Nonat, C. Allain, T. Gunnlaugsson, Inorg. Chem. 49 (2010) 8449.

[22] P. Coppo, M. Duati, V. N. Kozhevnikov, Jo. W. Hofstraat, L. De Cola, Angew. Chem. Int. Ed. 44 (2005) 1806.

[23] F. Chen, Z. Bian, Z. Liu, D. Nie, Z. Chen, C. Huang, Inorg. Chem. 47 (2008) 2507.

[24] A. Baschieri, S. Muzzioli, E. Matteucci, S. Stagni, M. Massi, L. Sambri, Dalton Trans. 44 (2015) 37.

[25] (a) E. Buckley-Dhoot, J. Fawcett, R. A. Kresinski, A. W. G. Platt, Polyhedron 28 (2009) 1497; (b) M. Yong-xiang, H. Guo-sheng, J. Pei-song, H. Xiao-jun, Bull. Soc. Chim. Belg. 100 (1991) 205; (c) W. Huang, J. L. Brosmer, P. L. Diaconescu, New J. Chem. 39 (2015) 7696; (d) V. Mereacre, A. M. Ako, G. Filoti, J. Bartolomé, C. E. Anson, A. K. Powell, Polyhedron 29 (2010) 244.

[26] (a) P. S. Koroteev, Zh. V. Dobrokhotova, N. N. Efimov, A. B. Ilyukhin, V. M. Novotortsev, Russian J. Coord. Chem. 40 (2014) 395; (b) L.-L. Huang, X.-Z. Han, Y.-M. Yao, Y. Zhang, Q. Shen, Appl. Organometal. Chem. 25 (2011) 464; (c) X.-Y. Gu, X.-Z. Han, Y.M. Yao, Y. Zhang, Q. Shen, J. Organomet. Chem. 695 (2010) 2726.

[27] Y. Yuan, T. Cardinaels, K. Lunstroot, K. Van Hecke, L. Van Meervelt, C. Gŏrller-Walrand,

K. Binnemans, P. Nockemann, Inorg. Chem. 46 (2007) 5302.

[28] S. Faulkner, M. Tropiano, N. L. Kilah, M. Morten, H. Rahman, J. J. Davis, P. D. Beer, J.Am. Chem. Soc. 133 (2011) 11847.

[29] T. D. W. Claridge, High-Resolution NMR Techniques in Organic Chemistry, Tetrahedron Organic Chemistry Series, Vol. 27, Elsevier, 2009.

[30] C. Y. Lin, M. W. George, P. M. W. Gill, Aust. J. Chem. 57 (2004) 365.

[31] W. J. Hehre, R. Ditchfield, J. A. Pople, J. Chem. Phys. 56 (1972) 2257.

[32] F. Jensen, Introduction to Computational Chemistry, second ed., Wiley and Sons Ed., Chichester, 2007.

[33] (a) Spartan '16, build 1.1.0, Wavefun Inc., Irvine CA; (b) Y. Shao, et al., Mol. Phys. 113 (2015) 184.

[34] D. D. Perrin, W. L. F. Armarego, Purification of Laboratory Chemicals, 3rd ed., Pergamon Press (1988).

[35] I. A. Golubeva, T. P. Vishnyakova, N. N. Bul'on, Synthesis of ferrocenecarboxylic acids and their derivates, Istitute of the Petrochemical and Gas Industry, n° 72, 61-67, 1967, (Moscow).

[36] S. Trofimenko, J. Am. Chem. Soc. 89 (1967) 6288.

[37] P. E. Fanta, Org. Synth. 32 (1952) 95.

[38] S. Trofimenko, *J. Org. Chem.* 28 (1963) 3243.

[39] W. C. (Ina) du Plessis, T. G. Vosloo, J. C. Swarts, J. Chem. Soc, Dalton Trans (1998) 2507-2514.

[40] I. Bertini, C. Luchinat, Coord. Chem. Rev. 150 (1996).

[41] S. Onuma, H. Inoue, S. Shibata, Bull. Chem. Soc. Jpn. 49 (1976) 644.

[42] M. E. N. P. R. A. Silva, A. J. L. Pombeiro, J. J. R. Fraústo da Silva, R. Herrmann, N. Deus, R. E. Bozak, J. Organomet. Chem. 480 (1994) 81.

[43] A. J. Bard, L. R. Faulkner, Electrochemical Methods, 2nd Ed., Wiley, New York, 2001.

[44] S. Fery-Forgues, B. Delavaux-Nicot, J. Photochem. Photobiol. A 132 (2000) 137.

[45] J.-C. G. Bünzli, S. V. Eliseeva, Basics of Lanthanide Photophysics, Springer-Verlag, Berlin, 2010

[46] (a) W. G. Herkstroeter, J. Am. Chem. Soc. 97 (1975) 4161; (b) M. Kikuchi, K. Kikuchi, H. Kokubun, Bull. Chem. Soc. Jpn. 47 (1974) 1331.

[47] L. Taffarel, Master Thesis, Ca' Foscari University, 2015.

[48] K. Binnemans, “Rare Earths Beta Diketonates” in Handbook on the Physics and Chemistry of Rare Earths, Vol. 35, eds. K. A. Gschneidner, Jr., J.-C. G. Bünzli and V. K. Pecharsky, Elsevier, Amsterdam, 2005, Chapter 225, pp. 107-272.

[49] (a) G. Gheno, M. Bortoluzzi, R. Ganzerla and F. Enrichi, J. Lumin. 145 (2014) 963; (b) M. Bortoluzzi, G. Paolucci, D. Fregona, L. Dalla Via and F. Enrichi, J. Coord. Chem. 65 (2012) 3903; (c) M. Bortoluzzi, G. Paolucci, M. Gatto, S. Roppa, F. Enrichi, S. Ciorba and B. S. Richards, J. Lumin.132 (2012) 2378; (d) M. Bortoluzzi, G. Paolucci, S. Polizzi, L. Bellotto, F. Enrichi, S. Ciorba and B. S. Richards, Inorg. Chem. Commun. 14 (2011) 1762.

[50] N. Marques, A. Sella, J. Takats, Chem. Rev. 102 (2002) 2137.

[51] (a) S.K. Ramalingam, S. Soundararajan, J. Inorg. Nucl. Chem. 29 (1967) 1763; (b) V.N. Krishnamurthy, S. Soundararajan, J. Inorg. Nucl. Chem. 29 (1967) 517; S. Ramalingam, S. Soundararajan, Z. Anorg. Allg. Chem. 353 (1967) 216.

[52] (a) M. Bortoluzzi, E. Bianchin, S. Roppa, V. Bertolasi, F. Enrichi, Dalton Trans, 43 (2014) 10120; (b) M. Bortoluzzi, D. Battistel, S. Roppa, S. Daniele, A. Perosa, F. Enrichi, Dalton Trans 43 (2014) 9303.